

This is an Open Access document downloaded from ORCA, Cardiff University's institutional repository: <https://orca.cardiff.ac.uk/id/eprint/149771/>

This is the author's version of a work that was submitted to / accepted for publication.

Citation for final published version:

Chen, Xiaodong, Nie, Guojun and Wu, Zhangming 2022. Global buckling and wrinkling of variable angle tow composite sandwich plates by a modified extended high-order sandwich plate theory. *Composite Structures* 292 , 115639. 10.1016/j.compstruct.2022.115639

Publishers page: <https://doi.org/10.1016/j.compstruct.2022.115639>

Please note:

Changes made as a result of publishing processes such as copy-editing, formatting and page numbers may not be reflected in this version. For the definitive version of this publication, please refer to the published source. You are advised to consult the publisher's version if you wish to cite this paper.

This version is being made available in accordance with publisher policies. See <http://orca.cf.ac.uk/policies.html> for usage policies. Copyright and moral rights for publications made available in ORCA are retained by the copyright holders.



Global buckling and wrinkling of variable angle tow composite sandwich plates by a modified extended high-order sandwich plate theory

Xiaodong Chen^{1,*} Guojun Nie^{2,†} Zhangming Wu^{3,4,‡}

¹ School of Civil and Transportation Engineering, Henan University of Urban Construction, Pingdingshan 467000, China

² School of Aerospace Engineering and Applied Mechanics, Tongji University, Shanghai 200092, China

³ School of Mechanical Engineering and Mechanics, Ningbo University, Ningbo 315211, China

⁴ Cardiff School of Engineering, Cardiff University, Cardiff CF24 3AA, UK

Abstract

The advanced Automated Fibre Placement (AFP) manufacturing technologies make the synthesis of Variable Angle Tow (VAT) composites, which enable the design of lightweight sandwich structures to possess variable stiffness facesheets. However, both global and local instability phenomena of VAT sandwich plates under in-plane compressive loads are rarely explored till now. The objective of this article is to fill this gap by developing a Rayleigh-Ritz procedure based on a modified extended high-order sandwich plate theory (EHSAPT). The original two-dimensional EHSAPT proposed by Phan et al. [1] is extended to a three-dimensional case with a minor modification that the first-order shear deformation theory instead of the classical Kirchhoff–Love hypothesis is adopted for each facesheet, which brings several merits such as the conciseness in derivation process and the easiness in program implementation. The Rayleigh-Ritz approach combined with the principle of minimum potential energy is employed to derive the eigenvalue equation that governs the instability problem of VAT sandwich plates under in-plane compressive loads. Both global buckling and wrinkling patterns of VAT sandwich plates can be captured under this proposed analytical model framework. Before instability analysis, the nonuniform prebuckling stresses over the entire sandwich plate are determined under the assumption of membrane prebuckling state. The usage of Lagrange multiplier method in the prebuck-

*E-mail address: 1263895177@qq.com (Xiaodong Chen, Corresponding author)

†E-mail address: ngj@tongji.edu.cn (Guojun Nie)

‡E-mail address: wuzhangming@nbu.edu.cn; wuz12@cardiff.ac.uk (Zhangming Wu)

ling regime removes the restrictions inherent in conventional Rayleigh-Ritz formulation and thus provides a general way to model in-plane boundary conditions. The accuracy and effectiveness of the developed Rayleigh-Ritz procedure are validated by comparing with previously published results and FE solutions given by ABAQUS. Effects of core thickness, core orthotropy, and fibre orientation angle of the facesheets on the instability behaviour of VAT sandwich plates are investigated. Finally, the mechanism of steering the fibre trajectory over the facesheets to improve the buckling resistance for the sandwich plate is studied and discussed.

Keywords: Global buckling, Wrinkling, Variable angle tow, Sandwich plate, EHSAPT, Rayleigh-Ritz method

Nomenclature

θ	fibre orientation angle
ϕ	rotation angle of the fibre path
T_0	fibre orientation angle at the starting point
T_1	fibre orientation angle at the ending point
a	plate length
b	plate width
h	plate thickness
f_t	thickness of the top facesheet
f_b	thickness of the bottom facesheet
$2c$	core thickness
$u^{t,b,c}$	displacement of a point in the x direction
$v^{t,b,c}$	displacement of a point in the y direction
$w^{t,b,c}$	displacement of a point in the z direction
$u_0^{t,b,c}$	in-plane displacement of the mid-plane in the x direction

$v_0^{t,b,c}$	in-plane displacement of the mid-plane in the y direction
$w_0^{t,b,c}$	out-of-plane displacement of the mid-plane
$\phi_{x0}^{t,b,c}$	rotation about the y axis of the mid-plane
$\phi_{y0}^{t,b,c}$	rotation about the x axis of the mid-plane
$\sigma_{ij}^{t,b,c}$	normal stress
$\tau_{ij}^{t,b,c}$	shear stress
$\varepsilon_{ij}^{t,b,c}$	normal strain
$\gamma_{ij}^{t,b,c}$	shear strain
$N_{ij}^{t,b}$	in-plane force resultant of the facesheet
$M_{ij}^{t,b}$	moment resultant of the facesheet
$A_{ij}^{t,b}$	extensional stiffness of the facesheet
$B_{ij}^{t,b}$	coupling stiffness of the facesheet
$D_{ij}^{t,b}$	bending stiffness of the facesheet
C_{ij}	stiffness coefficient of the core
U	strain energy
V	virtual work
L_n	the n^{th} Legendre polynomial
Φ	Airy's stress function
Λ_j^i	boundary stress coefficient
χ_j^i	Lagrange multiplier
\mathbb{L}_A	Lagrange function
Π_{LM}^*	stress constraint function
Π_{D}^*	displacement constraint function

1. Introduction

Sandwich structures are typically constructed by two thin and stiff facesheets and a thick and compliant core, which form an integrated structure with high strength, low weight and strong durability. Due to these outstanding features, sandwich structures have received many applications in aerospace, civil, marine, electronic and biomedical fields [2]. Traditionally, the facesheets of a sandwich plate are made of metal materials or straight-fibre composite laminates. Recently, the advent of variable angle tow composite laminates by advanced automated fibre placement technologies enables the design of novel sandwich plates with variable stiffness facesheets [3, 4]. This novel design concept for sandwich plates may provide designers a considerably large stiffness tailoring flexibility to design lightweight sandwich structures with superior performance. On the other hand, the variable stiffness property inherent in this novel type of sandwich plate structures often gives rise to significant challenges in the modelling and analysis. Therefore, there remains ongoing interests to develop an efficient and accurate analytical model for the analysis of the instability behaviours of VAT sandwich plates.

Generally, the instability behaviours of sandwich plates subjected to in-plane compression can be classified into two different types, that is, global or overall buckling and local buckling (wrinkling) [5, 6, 7]. The former is characterized by the large half-wavelength with the same order of magnitude of the in-plane dimension; whilst the latter is characterized by the short half-wavelength that is comparable to the plate thickness [8]. Under certain circumstances, such as in the deep post-buckling regime, these global and local instabilities may interact with each other and finally lead to complex failure forms [9, 10, 11, 12, 13]. Many methods have been developed to study these complex instability phenomena of sandwich plate structures. Early works [14, 15, 16] on instability analysis of sandwich structures considered global and local buckling models separately, namely, uncoupled approach. Afterwards, global buckling of the sandwich structure was studied based on the Equivalent Single-layer Theory (EST) or Layer Wise Theory (LWT) by a large number of researchers [2, 17], while wrinkling was investigated based on various elastic foundation model by relatively few researchers [18, 8]. On the other hand, the coupled approach was also introduced by many researchers to study both global buckling and wrinkling of sandwich plates and their interactions. For instance, Frostig et al. [19] proposed a high-order sandwich plate theory (HSAPT) based on the variational principle

and perform a rigorous buckling analysis of sandwich beams with soft cores. In their work, the soft core exhibits both the transverse flexibility and the shear resistance but is free of longitudinal normal stresses. By replacing the constant shear stress in the core [20, 19] with the gradient of rotation, Léotoing et al. [21] developed a novel unified model using five displacement variables to analyze both local and global instabilities of sandwich columns. In their works, the transverse and in-plane displacements in the core are represented by second-order and third-order polynomials with respect to plate thickness, respectively. Furthermore, the kinematics proposed by Léotoing et al. [21] has been implemented into FE model for the analysis of both global and local instability phenomena in sandwich structures [6, 22, 11, 23, 24, 13]. However, these sandwich models neglect the in-plane rigidity of the core. This assumption is only valid for soft cores, since the elastic modulus and flexural rigidity of the soft core are about three and two orders smaller than those of the facesheets, respectively [1]. Recently, Phan et al. [1] proposed an extension of the HSAPT, termed as EHSAPT, to model sandwich beams, in which the transverse compressibility, shear resistance and in-plane rigidity of the core are taken into account, simultaneously. Several research works [25, 26, 27, 28, 12] have adopted the fundamental modelling strategy of EHSAPT to study the instability problem of sandwich structures. It is worth noting that there exists a large difference between HSAPT/EHSAPT and HSDT (Higher-order Shear Deformation Theory) [29, 30, 31, 32] in terms of theoretical formulation and practical application. The former one is similar to the LWT, while the latter is considered as one of the ESTs. Other coupled approaches for the study of both global and local instability responses of the sandwich structure can be found in [33, 34, 35, 36, 37]. Among these sandwich plate models, it is worth highlighting the Carrera's Unified Formulation (CUF) proposed by Carrera [38, 39] and the Generalized Unified Formulation (GUF) developed by Demasi [40, 41]. Following the pioneering works by Carrera and Demasi, D'Ottavio et al. [7] developed a variable kinematic model, which is a sublaminar version of the GUF, termed as S-GUF. In their works, an assessment of several well known sandwich plate models for the global and local buckling analysis was presented. Recently, Vescovini et al. [42] applied the S-GUF approach to study both global and local buckling responses of anisotropic sandwich plates.

From the literature survey, it is evident that the research works on both global buckling and wrinkling analysis mainly focused on conventional sandwich plate structures. Up to

now, however, research works for instability analysis of VAT sandwich structures are very limited. Coburn and Weaver [3] developed a semi-analytical model based on the Ritz energy method for buckling analysis of VAT sandwich plates under in-plane compressive loads. In their work, the proposed buckling model fails to capture the facesheet wrinkling mode due to the fact that the core is assumed to be infinitely rigid (incompressible) along the thickness direction under the framework of the EST. Therefore, developing a more accurate model for both the global and local instability analysis of this novel type of sandwich structures remains necessary. To the best of the authors' knowledge, the instability problem of VAT sandwich plates occurring under in-plane compressive loads has not been well studied by using a coupled sandwich plate model. In this work, an efficient and accurate analytical model based on a modified version of the EHSAPT for analyzing both global buckling and wrinkling behaviours of VAT sandwich plates is developed. Although a considerable amount of research efforts [43, 44, 45, 46, 47, 48, 49, 50, 51, 52, 53] have been devoted to the study of buckling behaviour of VAT laminated plates, and the mechanism behind the significant improvement in the buckling resistance of VAT laminates had been well understood, the study of VAT sandwich plates is very limited. In view of this, this work aims to further study the mechanics of VAT sandwich plates and investigate the mechanism of applying VAT concept to improve the buckling performance for sandwich plates.

In the present work, an efficient and accurate Rayleigh-Ritz model based on a modified version of the EHSAPT is developed to study the instability problem of VAT sandwich plates under in-plane compressive loads. The original two-dimensional EHSAPT proposed by Phan et al. [1] is extended to a three-dimensional case with a minor modification that the first-order shear deformation theory instead of the classical Kirchhoff–Love hypothesis is adopted for each facesheet, which brings several merits such as the conciseness in derivation process and the easiness in program implementation. The Rayleigh-Ritz approach combined with the principle of minimum potential energy is employed to derive the eigenvalue equation that governs the instability problem of VAT sandwich plates. Both global buckling and wrinkling patterns can be captured under the proposed Rayleigh-Ritz analytical model. Before instability analysis, the nonuniform prebuckling stresses over the entire sandwich plate are determined under the assumption of membrane prebuckling state. The usage of Lagrange multiplier method in the prebuckling analysis removes

the restrictions inherent in conventional Rayleigh-Ritz formulation and thus provides a general way to model in-plane boundary conditions.

The remainder of this work is organized as follows: In the next section, the concept of VAT facesheets is introduced. Section 3 presents a theoretical formulation for the instability problem of VAT sandwich plates under in-plane compressive loads. In Section 4, the nonuniform prebuckling stresses of sandwich plates are determined using Rayleigh-Ritz formulation enhanced with Lagrange multiplier method under the assumption of membrane prebuckling state. In Section 5, the accuracy and effectiveness of the proposed Rayleigh-Ritz model for VAT sandwich plates are verified by a series of computational cases. Effects of core thickness, core orthotropy, and fibre orientation angle of the facesheets on the instability behaviours of VAT sandwich plates are analyzed and discussed by numerical examples. Finally, some conclusions are drawn in Section 6.

2. VAT facesheets

The orientation of fibre angles of each ply of the facesheets within the sandwich plate are continuously varied with respect to the coordinates x and y , which result in the variable stiffness properties. As such, VAT facesheets provide an extended stiffness tailoring flexibility for the design of the structural performance of sandwich plates. Generally, the fibre angle variation over the facesheets can be represented in a mathematical form using a small number of fibre angle parameters [44]. For the sake of simplicity, the facesheet with a linear fibre angle variation is considered in the present work, and the angle variation along the x' direction is given by [43],

$$\theta(x') = \phi + \frac{(T_1 - T_0)}{d} |x'| + T_0 \quad \text{with} \quad x' = x \cos \phi + y \sin \phi \quad (1)$$

where T_0 and T_1 are fibre orientation angles at two prescribed reference points; d is the distance between the starting and ending points; ϕ is the angle of rotation of the fibre path, which is chosen to be 0° and 90° in the present work such that d takes the half of the panel length (when $\phi = 0^\circ$) or width (when $\phi = 90^\circ$). The layup configuration for the tow-steered facesheet of the sandwich plate can be characterised by $[\phi \langle T_0 | T_1 \rangle]$. Fig. 1 illustrates a two-layers VAT facesheet $[0 \pm \langle 0 | 75 \rangle]$ with a linear variation of fibre orientation angle, in which $\phi = 0^\circ$, $T_0 = 0^\circ$, and $T_1 = 75^\circ$.

3. Theoretical formulation

3.1. Displacements and strains

As shown in Fig. 2, a rectangular sandwich plate of length a and width b with a core of thickness $2c$ is considered. The thicknesses of the top and bottom facesheets are f_t and f_b , respectively. Herein, both top and bottom facesheets are constructed by the VAT laminates, and thus exhibit variable stiffness properties. An orthogonal coordinate system located in the centroid of the core is introduced to establish the kinematic model, in which x and y respectively represent the length and width direction of the sandwich plate and z denotes the thickness direction normal to the mid-plane of the core. In the present work, the displacement field of the top and bottom facesheets is constructed based on the first-order shear deformation theory instead of the Kirchhoff–Love thin plate theory as done by Phan et al. [1]. The displacement field (u^t , v^t and w^t) for the top facesheet is then given by [54],

$$\begin{aligned} u^t(x, y, z) &= u_0^t(x, y) + (z - c - \frac{f_t}{2})\phi_{x0}^t(x, y) \\ v^t(x, y, z) &= v_0^t(x, y) + (z - c - \frac{f_t}{2})\phi_{y0}^t(x, y) \\ w^t(x, y, z) &= w_0^t(x, y) \end{aligned} \quad (2)$$

with $c \leq z \leq c + f_t$, while the displacement field (u^b , v^b and w^b) for the bottom facesheet is denoted as

$$\begin{aligned} u^b(x, y, z) &= u_0^b(x, y) + (z + c + \frac{f_b}{2})\phi_{x0}^b(x, y) \\ v^b(x, y, z) &= v_0^b(x, y) + (z + c + \frac{f_b}{2})\phi_{y0}^b(x, y) \\ w^b(x, y, z) &= w_0^b(x, y) \end{aligned} \quad (3)$$

with $-c - f_b \leq z \leq -c$. Herein, $u_0^{t,b}$, $v_0^{t,b}$ and $w_0^{t,b}$ represent the in-plane and out-of-plane displacement components of a point on the mid-plane of each facesheet, respectively; $\phi_{x0}^{t,b}$ and $\phi_{y0}^{t,b}$ are the rotation of a transverse normal about the y - and x -axis on the mid-plane of each facesheet, respectively. On the other hand, in order to capture the complex behaviour of instability, the displacement field (u^c , v^c and w^c) of the core requires to be enriched by using a high-order sandwich plate theory. In the present work, the original two-dimensional EHSAPT theory proposed by Phan et al. [1] is extended to

a three-dimensional model, in which the transverse compressibility, shear resistance as well as in-plane rigidity of the core are taken into account. According to the EHSAPT theory, the displacement field for the core is expressed as a cubic function for the in-plane displacements (u^c and v^c) and a quadratic function for the out-of-plane displacement (w^c),

$$\begin{aligned}
u^c(x, y, z) &= u_0^c(x, y) + \phi_{x0}^c(x, y)z + u_2^c(x, y)z^2 + u_3^c(x, y)z^3 \\
v^c(x, y, z) &= v_0^c(x, y) + \phi_{y0}^c(x, y)z + v_2^c(x, y)z^2 + v_3^c(x, y)z^3 \\
w^c(x, y, z) &= w_0^c(x, y) + w_1^c(x, y)z + w_2^c(x, y)z^2
\end{aligned} \tag{4}$$

with $-c \leq z \leq c$, where u_0^c , v_0^c and w_0^c are the in-plane and out-of-plane displacement components of a point on the mid-plane of the core, respectively; ϕ_{x0}^c and ϕ_{y0}^c are the rotations of a transverse normal about the y - and x -axis on the mid-plane of the core, respectively; u_2^c , u_3^c , v_2^c , v_3^c , w_1^c and w_2^c are the unknown functions that will be determined from the continuity conditions at the upper ($z = c$) and lower ($z = -c$) face-core interfaces, which are given as follows,

$$\begin{aligned}
u^t(x, y, c) &= u^c(x, y, c) \\
v^t(x, y, c) &= v^c(x, y, c) \\
w^t(x, y, c) &= w^c(x, y, c) \\
u^b(x, y, -c) &= u^c(x, y, -c) \\
v^b(x, y, -c) &= v^c(x, y, -c) \\
w^b(x, y, -c) &= w^c(x, y, -c)
\end{aligned} \tag{5}$$

Substituting Eqs. (2)-(4) into Eq. (5), one can directly obtain

$$\begin{aligned}
u_2^c(x, y) &= \frac{u_0^t(x, y) + u_0^b(x, y) - \frac{1}{2}f_t\phi_{x0}^t(x, y) + \frac{1}{2}f_b\phi_{x0}^b(x, y) - 2u_0^c(x, y)}{2c^2} \\
u_3^c(x, y) &= \frac{u_0^t(x, y) - u_0^b(x, y) - \frac{1}{2}f_t\phi_{x0}^t(x, y) - \frac{1}{2}f_b\phi_{x0}^b(x, y) - 2c\phi_{x0}^c(x, y)}{2c^3} \\
v_2^c(x, y) &= \frac{v_0^t(x, y) + v_0^b(x, y) - \frac{1}{2}f_t\phi_{y0}^t(x, y) + \frac{1}{2}f_b\phi_{y0}^b(x, y) - 2v_0^c(x, y)}{2c^2} \\
v_3^c(x, y) &= \frac{v_0^t(x, y) - v_0^b(x, y) - \frac{1}{2}f_t\phi_{y0}^t(x, y) - \frac{1}{2}f_b\phi_{y0}^b(x, y) - 2c\phi_{y0}^c(x, y)}{2c^3} \\
w_1^c(x, y) &= \frac{w_0^t(x, y) - w_0^b(x, y)}{2c} \\
w_2^c(x, y) &= \frac{w_0^t(x, y) + w_0^b(x, y) - 2w_0^c(x, y)}{2c^2}
\end{aligned} \tag{6}$$

and thus the displacement fields of a point within the core can be rewritten as

$$\begin{aligned}
u^c(x, y, z) &= \alpha_1 u_0^t(x, y) + \alpha_2 u_0^b(x, y) + \alpha_3 u_0^c(x, y) + \alpha_4 \phi_{x0}^t(x, y) + \alpha_5 \phi_{x0}^b(x, y) + \alpha_6 \phi_{x0}^c(x, y) \\
v^c(x, y, z) &= \alpha_1 v_0^t(x, y) + \alpha_2 v_0^b(x, y) + \alpha_3 v_0^c(x, y) + \alpha_4 \phi_{y0}^t(x, y) + \alpha_5 \phi_{y0}^b(x, y) + \alpha_6 \phi_{y0}^c(x, y) \\
w^c(x, y, z) &= \beta_1 w_0^t(x, y) + \beta_2 w_0^b(x, y) + \beta_3 w_0^c(x, y)
\end{aligned} \tag{7}$$

where

$$\begin{aligned}
\alpha_1 &= \frac{z^2}{2c^2} + \frac{z^3}{2c^3}; & \alpha_2 &= \frac{z^2}{2c^2} - \frac{z^3}{2c^3}; & \alpha_3 &= 1 - \frac{z^2}{c^2} \\
\alpha_4 &= -\frac{f_t}{2} \left(\frac{z^2}{2c^2} + \frac{z^3}{2c^3} \right); & \alpha_5 &= \frac{f_b}{2} \left(\frac{z^2}{2c^2} - \frac{z^3}{2c^3} \right); & \alpha_6 &= z \left(1 - \frac{z^2}{c^2} \right) \\
\beta_1 &= \frac{z}{2c} + \frac{z^2}{2c^2}; & \beta_2 &= -\frac{z}{2c} + \frac{z^2}{2c^2}; & \beta_3 &= 1 - \frac{z^2}{c^2}
\end{aligned} \tag{8}$$

It is worth highlighting that the in-plane displacement component (u^c or v^c) is only related to the in-plane displacements ($u_0^{t,b,c}$ or $v_0^{t,b,c}$) and the rotations ($\phi_{x0}^{t,b,c}$ or $\phi_{y0}^{t,b,c}$) on the mid-plane of both the facesheets and the core, whilst the vertical displacement component (w^c) is only associated with the out-of-plane displacements ($w_0^{t,b,c}$). From a mathematical point of view, the in-plane displacement component (u^c or v^c) of a point within the core can be considered as a linear combination of the in-plane displacements ($u_0^{t,b,c}$ or $v_0^{t,b,c}$) and the rotations ($\phi_{x0}^{t,b,c}$ or $\phi_{y0}^{t,b,c}$) with respect to the generalized coordinates α_i ($i = 1, 2, 3, 4, 5, 6$), while the vertical displacement component (w^c) can be represented as a linear combination of the out-of-plane displacements ($w_0^{t,b,c}$) with respect to the generalized coordinates β_j ($j = 1, 2, 3$). Due to the introduction of the rotation variables ($\phi_{x0}^{t,b}$ and $\phi_{y0}^{t,b}$) on the mid-plane of both the top and bottom facesheets as in Eqs. (2) and (3), **no coupling terms** appear in these displacement components (u^c , v^c and w^c) of a point within the core, which means that the displacement components within the core are independent with each other. It is noted that the modified EHSAPT will be degenerated into the original EHSAPT if substituting the following expressions into Eqs. (2) and (3),

$$\phi_{x0}^{t,b} = -\frac{\partial w_0^{t,b}}{\partial x}; \quad \phi_{y0}^{t,b} = -\frac{\partial w_0^{t,b}}{\partial y} \tag{9}$$

However, the existing of coupling terms in the original EHSAPT theory results in higher order derivatives in Eq. (7), which lead to a tedious formula derivation process and

further increases the difficulty for program implementation, albeit it has the merits such as fewer unknown variables. The advantage of this modified EHSAPT lies in that it leads to a concise derivation process and a simple program implementation. In addition, this modified EHSAPT theory is also applicable to model the sandwich plates with moderately thick facesheets, as the FSDT is applied.

With the displacement fields defined in Eqs. (2) and (3), the linear terms of strains (ε_{xx}^t , ε_{yy}^t , γ_{yz}^t , γ_{xz}^t and γ_{xy}^t) for the top facesheet are expressed as [54]

$$\begin{Bmatrix} \varepsilon_{xx}^t \\ \varepsilon_{yy}^t \\ \gamma_{yz}^t \\ \gamma_{xz}^t \\ \gamma_{xy}^t \end{Bmatrix} = \begin{Bmatrix} \frac{\partial u^t}{\partial x} \\ \frac{\partial v^t}{\partial y} \\ \frac{\partial v^t}{\partial z} + \frac{\partial w^t}{\partial y} \\ \frac{\partial u^t}{\partial z} + \frac{\partial w^t}{\partial x} \\ \frac{\partial u^t}{\partial y} + \frac{\partial v^t}{\partial x} \end{Bmatrix} = \begin{Bmatrix} \varepsilon_{xx}^{t(0)} \\ \varepsilon_{yy}^{t(0)} \\ \gamma_{yz}^{t(0)} \\ \gamma_{xz}^{t(0)} \\ \gamma_{xy}^{t(0)} \end{Bmatrix} + (z - c - \frac{f_t}{2}) \begin{Bmatrix} \varepsilon_{xx}^{t(1)} \\ \varepsilon_{yy}^{t(1)} \\ 0 \\ 0 \\ \gamma_{xy}^{t(1)} \end{Bmatrix}; \quad c \leq z \leq c + f_t \quad (10)$$

and similarly, the strains (ε_{xx}^b , ε_{yy}^b , γ_{yz}^b , γ_{xz}^b and γ_{xy}^b) of the bottom facesheet are given by [54]

$$\begin{Bmatrix} \varepsilon_{xx}^b \\ \varepsilon_{yy}^b \\ \gamma_{yz}^b \\ \gamma_{xz}^b \\ \gamma_{xy}^b \end{Bmatrix} = \begin{Bmatrix} \frac{\partial u^b}{\partial x} \\ \frac{\partial v^b}{\partial y} \\ \frac{\partial v^b}{\partial z} + \frac{\partial w^b}{\partial y} \\ \frac{\partial u^b}{\partial z} + \frac{\partial w^b}{\partial x} \\ \frac{\partial u^b}{\partial y} + \frac{\partial v^b}{\partial x} \end{Bmatrix} = \begin{Bmatrix} \varepsilon_{xx}^{b(0)} \\ \varepsilon_{yy}^{b(0)} \\ \gamma_{yz}^{b(0)} \\ \gamma_{xz}^{b(0)} \\ \gamma_{xy}^{b(0)} \end{Bmatrix} + (z + c + \frac{f_b}{2}) \begin{Bmatrix} \varepsilon_{xx}^{b(1)} \\ \varepsilon_{yy}^{b(1)} \\ 0 \\ 0 \\ \gamma_{xy}^{b(1)} \end{Bmatrix}; \quad -c - f_b \leq z \leq -c \quad (11)$$

with

$$\begin{aligned} \varepsilon_{xx}^{t,b(0)} &= \frac{\partial u_0^{t,b}}{\partial x}; & \varepsilon_{xx}^{t,b(1)} &= \frac{\partial \phi_{x0}^{t,b}}{\partial x} \\ \varepsilon_{yy}^{t,b(0)} &= \frac{\partial v_0^{t,b}}{\partial y}; & \varepsilon_{yy}^{t,b(1)} &= \frac{\partial \phi_{y0}^{t,b}}{\partial y} \\ \gamma_{yz}^{t,b(0)} &= \phi_{y0}^{t,b} + \frac{\partial w_0^{t,b}}{\partial y}; & \gamma_{xz}^{t,b(0)} &= \phi_{x0}^{t,b} + \frac{\partial w_0^{t,b}}{\partial x} \\ \gamma_{xy}^{t,b(0)} &= \frac{\partial u_0^{t,b}}{\partial y} + \frac{\partial v_0^{t,b}}{\partial x}; & \gamma_{xy}^{t,b(1)} &= \frac{\partial \phi_{x0}^{t,b}}{\partial y} + \frac{\partial \phi_{y0}^{t,b}}{\partial x} \end{aligned} \quad (12)$$

Moreover, the strains (ε_{xx}^c , ε_{yy}^c , ε_{zz}^c , γ_{yz}^c , γ_{xz}^c and γ_{xy}^c) of the core can be expressed as [54]

$$\begin{pmatrix} \varepsilon_{xx}^c \\ \varepsilon_{yy}^c \\ \varepsilon_{zz}^c \\ \gamma_{yz}^c \\ \gamma_{xz}^c \\ \gamma_{xy}^c \end{pmatrix} = \begin{pmatrix} \frac{\partial u^c}{\partial x} \\ \frac{\partial v^c}{\partial y} \\ \frac{\partial w^c}{\partial z} \\ \frac{\partial v^c}{\partial z} + \frac{\partial w^c}{\partial y} \\ \frac{\partial u^c}{\partial z} + \frac{\partial w^c}{\partial x} \\ \frac{\partial u^c}{\partial y} + \frac{\partial v^c}{\partial x} \end{pmatrix} \quad (13)$$

with

$$\begin{aligned} \frac{\partial u^c}{\partial x} &= \alpha_1 \frac{\partial u_0^t}{\partial x} + \alpha_2 \frac{\partial u_0^b}{\partial x} + \alpha_3 \frac{\partial u_0^c}{\partial x} + \alpha_4 \frac{\partial \phi_{x0}^t}{\partial x} + \alpha_5 \frac{\partial \phi_{x0}^b}{\partial x} + \alpha_6 \frac{\partial \phi_{x0}^c}{\partial x} \\ \frac{\partial v^c}{\partial x} &= \alpha_1 \frac{\partial v_0^t}{\partial x} + \alpha_2 \frac{\partial v_0^b}{\partial x} + \alpha_3 \frac{\partial v_0^c}{\partial x} + \alpha_4 \frac{\partial \phi_{y0}^t}{\partial x} + \alpha_5 \frac{\partial \phi_{y0}^b}{\partial x} + \alpha_6 \frac{\partial \phi_{y0}^c}{\partial x} \\ \frac{\partial w^c}{\partial x} &= \beta_1 \frac{\partial w_0^t}{\partial x} + \beta_2 \frac{\partial w_0^b}{\partial x} + \beta_3 \frac{\partial w_0^c}{\partial x} \\ \frac{\partial u^c}{\partial y} &= \alpha_1 \frac{\partial u_0^t}{\partial y} + \alpha_2 \frac{\partial u_0^b}{\partial y} + \alpha_3 \frac{\partial u_0^c}{\partial y} + \alpha_4 \frac{\partial \phi_{x0}^t}{\partial y} + \alpha_5 \frac{\partial \phi_{x0}^b}{\partial y} + \alpha_6 \frac{\partial \phi_{x0}^c}{\partial y} \\ \frac{\partial v^c}{\partial y} &= \alpha_1 \frac{\partial v_0^t}{\partial y} + \alpha_2 \frac{\partial v_0^b}{\partial y} + \alpha_3 \frac{\partial v_0^c}{\partial y} + \alpha_4 \frac{\partial \phi_{y0}^t}{\partial y} + \alpha_5 \frac{\partial \phi_{y0}^b}{\partial y} + \alpha_6 \frac{\partial \phi_{y0}^c}{\partial y} \\ \frac{\partial w^c}{\partial y} &= \beta_1 \frac{\partial w_0^t}{\partial y} + \beta_2 \frac{\partial w_0^b}{\partial y} + \beta_3 \frac{\partial w_0^c}{\partial y} \\ \frac{\partial u^c}{\partial z} &= \alpha_1' u_0^t + \alpha_2' u_0^b + \alpha_3' u_0^c + \alpha_4' \phi_{x0}^t + \alpha_5' \phi_{x0}^b + \alpha_6' \phi_{x0}^c \\ \frac{\partial v^c}{\partial z} &= \alpha_1' v_0^t + \alpha_2' v_0^b + \alpha_3' v_0^c + \alpha_4' \phi_{y0}^t + \alpha_5' \phi_{y0}^b + \alpha_6' \phi_{y0}^c \\ \frac{\partial w^c}{\partial z} &= \beta_1' w_0^t + \beta_2' w_0^b + \beta_3' w_0^c \end{aligned} \quad (14)$$

where the symbol $'$ denotes the first-order derivative with respect to z . It is clear that the lower-order derivatives that appear in Eq. (14) are due to the introduction of the rotation variables ($\phi_{x0}^{t,b}$ and $\phi_{y0}^{t,b}$) on the mid-plane of both the top and bottom facesheets.

3.2. Constitutive equations

Following the first-order shear deformation theory, the relationships between the stresses ($\sigma_{xx}^{t,b}$, $\sigma_{yy}^{t,b}$, $\tau_{yz}^{t,b}$, $\tau_{xz}^{t,b}$ and $\tau_{xy}^{t,b}$) and the strains ($\varepsilon_{xx}^{t,b}$, $\varepsilon_{yy}^{t,b}$, $\gamma_{yz}^{t,b}$, $\gamma_{xz}^{t,b}$ and $\gamma_{xy}^{t,b}$) of each lamina

within either the top or bottom VAT facesheet are expressed as [54]

$$\begin{Bmatrix} \sigma_{xx}^{t,b} \\ \sigma_{yy}^{t,b} \\ \tau_{xy}^{t,b} \end{Bmatrix}^{(k)} = \begin{bmatrix} Q_{11}^{t,b}(x,y) & Q_{12}^{t,b}(x,y) & Q_{16}^{t,b}(x,y) \\ Q_{12}^{t,b}(x,y) & Q_{22}^{t,b}(x,y) & Q_{26}^{t,b}(x,y) \\ Q_{16}^{t,b}(x,y) & Q_{26}^{t,b}(x,y) & Q_{66}^{t,b}(x,y) \end{bmatrix}^{(k)} \begin{Bmatrix} \varepsilon_{xx}^{t,b} \\ \varepsilon_{yy}^{t,b} \\ \gamma_{xy}^{t,b} \end{Bmatrix} \quad (15a)$$

$$\begin{Bmatrix} \tau_{yz}^{t,b} \\ \tau_{xz}^{t,b} \end{Bmatrix}^{(k)} = \begin{bmatrix} Q_{44}^{t,b}(x,y) & Q_{45}^{t,b}(x,y) \\ Q_{45}^{t,b}(x,y) & Q_{55}^{t,b}(x,y) \end{bmatrix}^{(k)} \begin{Bmatrix} \gamma_{yz}^{t,b} \\ \gamma_{xz}^{t,b} \end{Bmatrix} \quad (15b)$$

where $Q_{ij}^{t,b}$ ($i, j = 1, 2, 6$ or $i, j = 4, 5$) are the transformed material stiffnesses of the k^{th} layer within the VAT top or bottom facesheet, which vary with the position over the plate domain. In this work, the core is assumed to be a three-dimensional, orthotropic solid body, in which the occurrence of buckling will cause the warping of core cross-sections and the change of core thickness [25, 26]. Therefore, the stress-strain relationship of the core within the VAT composite sandwich plate can be written as [54],

$$\begin{Bmatrix} \sigma_{xx}^c \\ \sigma_{yy}^c \\ \sigma_{zz}^c \\ \tau_{yz}^c \\ \tau_{xz}^c \\ \tau_{xy}^c \end{Bmatrix} = \begin{bmatrix} C_{11} & C_{12} & C_{13} & 0 & 0 & 0 \\ C_{12} & C_{22} & C_{23} & 0 & 0 & 0 \\ C_{13} & C_{23} & C_{33} & 0 & 0 & 0 \\ 0 & 0 & 0 & C_{44} & 0 & 0 \\ 0 & 0 & 0 & 0 & C_{55} & 0 \\ 0 & 0 & 0 & 0 & 0 & C_{66} \end{bmatrix} \begin{Bmatrix} \varepsilon_{xx}^c \\ \varepsilon_{yy}^c \\ \varepsilon_{zz}^c \\ \gamma_{yz}^c \\ \gamma_{xz}^c \\ \gamma_{xy}^c \end{Bmatrix} \quad (16)$$

where C_{ij} ($i, j = 1, 2, 3, 4, 5, 6$) denotes stiffness coefficients, which are expressed in terms of engineering constants [54] :

$$\begin{aligned} C_{11} &= \frac{1 - \nu_{23}^c \nu_{32}^c}{E_{22}^c E_{33}^c \Delta}; & C_{12} &= \frac{\nu_{21}^c + \nu_{31}^c \nu_{23}^c}{E_{22}^c E_{33}^c \Delta}; & C_{13} &= \frac{\nu_{31}^c + \nu_{21}^c \nu_{32}^c}{E_{22}^c E_{33}^c \Delta} \\ C_{22} &= \frac{1 - \nu_{31}^c \nu_{13}^c}{E_{11}^c E_{33}^c \Delta}; & C_{23} &= \frac{\nu_{32}^c + \nu_{31}^c \nu_{12}^c}{E_{11}^c E_{33}^c \Delta}; & C_{33} &= \frac{1 - \nu_{12}^c \nu_{21}^c}{E_{11}^c E_{22}^c \Delta} \\ C_{44} &= G_{23}^c; & C_{55} &= G_{13}^c; & C_{66} &= G_{12}^c \\ \Delta &= \frac{1 - \nu_{12}^c \nu_{21}^c - \nu_{23}^c \nu_{32}^c - \nu_{31}^c \nu_{13}^c - 2\nu_{21}^c \nu_{32}^c \nu_{13}^c}{E_{11}^c E_{22}^c E_{33}^c} \end{aligned} \quad (17)$$

3.3. Governing equations

The governing equations for the instability problem of VAT sandwich plates are derived based on the principle of minimum potential energy, i.e., [54]

$$\delta\Pi = \delta U + \delta V = 0 \quad (18)$$

where δU denotes the variation of strain energy of the sandwich plate in a buckling state; δV is the variation of the virtual work done by in-plane loadings. Herein, the virtual strain energy δU contains the contributions from two facesheets and one core, that is,

$$\delta U = \delta U^t + \delta U^b + \delta U^c \quad (19)$$

with

$$\delta U^t = \iint_{\Omega} \left\{ \int_c^{c+f_t} [\sigma_{xx}^t \delta \varepsilon_{xx}^t + \sigma_{yy}^t \delta \varepsilon_{yy}^t + \tau_{yz}^t \delta \gamma_{yz}^t + \tau_{xz}^t \delta \gamma_{xz}^t + \tau_{xy}^t \delta \gamma_{xy}^t] dz \right\} dx dy \quad (20a)$$

$$\delta U^b = \iint_{\Omega} \left\{ \int_{-c-f_b}^{-c} [\sigma_{xx}^b \delta \varepsilon_{xx}^b + \sigma_{yy}^b \delta \varepsilon_{yy}^b + \tau_{yz}^b \delta \gamma_{yz}^b + \tau_{xz}^b \delta \gamma_{xz}^b + \tau_{xy}^b \delta \gamma_{xy}^b] dz \right\} dx dy \quad (20b)$$

$$\delta U^c = \iint_{\Omega} \left\{ \int_{-c}^c [\sigma_{xx}^c \delta \varepsilon_{xx}^c + \sigma_{yy}^c \delta \varepsilon_{yy}^c + \sigma_{zz}^c \delta \varepsilon_{zz}^c + \tau_{yz}^c \delta \gamma_{yz}^c + \tau_{xz}^c \delta \gamma_{xz}^c + \tau_{xy}^c \delta \gamma_{xy}^c] dz \right\} dx dy \quad (20c)$$

By substituting Eqs. (10), (11) and (15) into Eqs. (20a) and (20b), introducing the parameter $\bar{z} = z - c - \frac{f_t}{2}$ for the top facesheet or $\bar{z} = z + c + \frac{f_b}{2}$ for the bottom facesheet and integrating over \bar{z} through the thickness of $\bar{z} \in [-\frac{f_t}{2}, \frac{f_t}{2}]$ for top facesheet or $\bar{z} \in [-\frac{f_b}{2}, \frac{f_b}{2}]$ for bottom facesheet, we can obtain,

$$\begin{aligned} \delta U^t = \iint_{\Omega} \{ & N_{xx}^t \delta \varepsilon_{xx}^{t(0)} + N_{yy}^t \delta \varepsilon_{yy}^{t(0)} + N_{xy}^t \delta \gamma_{xy}^{t(0)} + M_{xx}^t \delta \varepsilon_{xx}^{t(1)} + M_{yy}^t \delta \varepsilon_{yy}^{t(1)} + M_{xy}^t \delta \gamma_{xy}^{t(1)} \\ & + Q_y^t \delta \gamma_{yz}^{t(0)} + Q_x^t \delta \gamma_{xz}^{t(0)} \} dx dy \end{aligned} \quad (21a)$$

$$\begin{aligned} \delta U^b = \iint_{\Omega} \{ & N_{xx}^b \delta \varepsilon_{xx}^{b(0)} + N_{yy}^b \delta \varepsilon_{yy}^{b(0)} + N_{xy}^b \delta \gamma_{xy}^{b(0)} + M_{xx}^b \delta \varepsilon_{xx}^{b(1)} + M_{yy}^b \delta \varepsilon_{yy}^{b(1)} + M_{xy}^b \delta \gamma_{xy}^{b(1)} \\ & + Q_y^b \delta \gamma_{yz}^{b(0)} + Q_x^b \delta \gamma_{xz}^{b(0)} \} dx dy \end{aligned} \quad (21b)$$

with

$$\begin{pmatrix} N_{xx}^{t,b} \\ N_{yy}^{t,b} \\ N_{xy}^{t,b} \\ M_{xx}^{t,b} \\ M_{yy}^{t,b} \\ M_{xy}^{t,b} \end{pmatrix} = \begin{bmatrix} A_{11}^{t,b}(x,y) & A_{12}^{t,b}(x,y) & A_{16}^{t,b}(x,y) & B_{11}^{t,b}(x,y) & B_{12}^{t,b}(x,y) & B_{16}^{t,b}(x,y) \\ A_{12}^{t,b}(x,y) & A_{22}^{t,b}(x,y) & A_{26}^{t,b}(x,y) & B_{12}^{t,b}(x,y) & B_{22}^{t,b}(x,y) & B_{26}^{t,b}(x,y) \\ A_{16}^{t,b}(x,y) & A_{26}^{t,b}(x,y) & A_{66}^{t,b}(x,y) & B_{16}^{t,b}(x,y) & B_{26}^{t,b}(x,y) & B_{66}^{t,b}(x,y) \\ B_{11}^{t,b}(x,y) & B_{12}^{t,b}(x,y) & B_{16}^{t,b}(x,y) & D_{11}^{t,b}(x,y) & D_{12}^{t,b}(x,y) & D_{16}^{t,b}(x,y) \\ B_{12}^{t,b}(x,y) & B_{22}^{t,b}(x,y) & B_{26}^{t,b}(x,y) & D_{12}^{t,b}(x,y) & D_{22}^{t,b}(x,y) & D_{26}^{t,b}(x,y) \\ B_{16}^{t,b}(x,y) & B_{26}^{t,b}(x,y) & B_{66}^{t,b}(x,y) & D_{16}^{t,b}(x,y) & D_{26}^{t,b}(x,y) & D_{66}^{t,b}(x,y) \end{bmatrix} \begin{pmatrix} \varepsilon_{xx}^{t,b(0)} \\ \varepsilon_{yy}^{t,b(0)} \\ \gamma_{xy}^{t,b(0)} \\ \varepsilon_{xx}^{t,b(1)} \\ \varepsilon_{yy}^{t,b(1)} \\ \gamma_{xy}^{t,b(1)} \end{pmatrix} \quad (22a)$$

$$\begin{pmatrix} Q_y^{t,b} \\ Q_x^{t,b} \end{pmatrix} = K \begin{bmatrix} A_{44}^{t,b}(x,y) & A_{45}^{t,b}(x,y) \\ A_{45}^{t,b}(x,y) & A_{55}^{t,b}(x,y) \end{bmatrix} \begin{pmatrix} \gamma_{yz}^{t,b(0)} \\ \gamma_{xz}^{t,b(0)} \end{pmatrix} \quad (22b)$$

where $N_{xx}^{t,b}$, $N_{yy}^{t,b}$ and $N_{xy}^{t,b}$ are the in-plane force resultants of either the top or bottom facesheet; $M_{xx}^{t,b}$, $M_{yy}^{t,b}$ and $M_{xy}^{t,b}$ are the moment resultants; $Q_y^{t,b}$ and $Q_x^{t,b}$ are the transverse force resultants; K denotes the shear correction factor, which depends on lamina properties and lamination scheme [54], and in the present work, K is chosen to be 5/6 [3]; $A_{ij}^{t,b}$, $B_{ij}^{t,b}$ and $D_{ij}^{t,b}$ ($i, j = 1, 2, 6$ or $i, j = 4, 5$) are the extensional, coupling and bending stiffness, respectively [54]. For VAT layups, each stiffness coefficient varies with the coordinates x and y over the plate domain $(x, y) \in [-\frac{a}{2}, \frac{a}{2}] \times [-\frac{b}{2}, \frac{b}{2}]$, which provides an extended flexibility for stiffness tailoring. In particular, if the VAT layups of the top or bottom facesheet is considered to be symmetric with respect to its respective mid-plane, the coupling stiffness terms will vanish in the constitutive relation given by Eq. (22a),

that is, $B_{ij}^{t,b} = 0$ ($i, j = 1, 2, 6$), and thus Eq. (22a) can be decoupled into,

$$\begin{Bmatrix} N_{xx}^{t,b} \\ N_{yy}^{t,b} \\ N_{xy}^{t,b} \end{Bmatrix} = \begin{bmatrix} A_{11}^{t,b}(x, y) & A_{12}^{t,b}(x, y) & A_{16}^{t,b}(x, y) \\ A_{12}^{t,b}(x, y) & A_{22}^{t,b}(x, y) & A_{26}^{t,b}(x, y) \\ A_{16}^{t,b}(x, y) & A_{26}^{t,b}(x, y) & A_{66}^{t,b}(x, y) \end{bmatrix} \begin{Bmatrix} \varepsilon_{xx}^{t,b(0)} \\ \varepsilon_{yy}^{t,b(0)} \\ \gamma_{xy}^{t,b(0)} \end{Bmatrix} \quad (23a)$$

$$\begin{Bmatrix} M_{xx}^{t,b} \\ M_{yy}^{t,b} \\ M_{xy}^{t,b} \end{Bmatrix} = \begin{bmatrix} D_{11}^{t,b}(x, y) & D_{12}^{t,b}(x, y) & D_{16}^{t,b}(x, y) \\ D_{12}^{t,b}(x, y) & D_{22}^{t,b}(x, y) & D_{26}^{t,b}(x, y) \\ D_{16}^{t,b}(x, y) & D_{26}^{t,b}(x, y) & D_{66}^{t,b}(x, y) \end{bmatrix} \begin{Bmatrix} \varepsilon_{xx}^{t,b(1)} \\ \varepsilon_{yy}^{t,b(1)} \\ \gamma_{xy}^{t,b(1)} \end{Bmatrix} \quad (23b)$$

Since the mid-plane symmetry of a composite layup that can eliminate the warping effect induced by cure during practical manufacturing is generally preferred, the symmetrical VAT composite laminates are employed to construct the two facesheets in the present work. In addition, it is worth highlighting that the above derivation process for either the top or bottom facesheet is very similar to that of the first-order shear deformation plate. Indeed, both the top and bottom facesheets within the VAT sandwich plate are independently deformed in its respective pattern and thus the local response of the entire sandwich plate can be captured.

On the other hand, the virtual work δV of the prebuckling stresses ($\widehat{N}_{xx}^{t,b,c}$, $\widehat{N}_{yy}^{t,b,c}$, $\widehat{N}_{xy}^{t,b,c}$) induced by in-plane loadings arises from their action on the corresponding second-order strains. Depending on whether considering the contribution of the core or not, the virtual work δV can be expressed as follows,

$$\delta V = \delta V^t + \delta V^b + \delta V^c \quad (24a)$$

$$\delta V = \delta V^t + \delta V^b \quad (24b)$$

In particular, if the von Kármán's second-order strains are considered, the components of

Eq. (24) are expanded as,

$$\begin{aligned}
\delta V^t &= -\widehat{N}_{xx}^t \frac{\partial w_0^t}{\partial x} \delta\left(\frac{\partial w_0^t}{\partial x}\right) - \widehat{N}_{yy}^t \frac{\partial w_0^t}{\partial y} \delta\left(\frac{\partial w_0^t}{\partial y}\right) - \widehat{N}_{xy}^t \frac{\partial w_0^t}{\partial x} \delta\left(\frac{\partial w_0^t}{\partial y}\right) - \widehat{N}_{xy}^t \frac{\partial w_0^t}{\partial y} \delta\left(\frac{\partial w_0^t}{\partial x}\right) \\
\delta V^b &= -\widehat{N}_{xx}^b \frac{\partial w_0^b}{\partial x} \delta\left(\frac{\partial w_0^b}{\partial x}\right) - \widehat{N}_{yy}^b \frac{\partial w_0^b}{\partial y} \delta\left(\frac{\partial w_0^b}{\partial y}\right) - \widehat{N}_{xy}^b \frac{\partial w_0^b}{\partial x} \delta\left(\frac{\partial w_0^b}{\partial y}\right) - \widehat{N}_{xy}^b \frac{\partial w_0^b}{\partial y} \delta\left(\frac{\partial w_0^b}{\partial x}\right) \\
\delta V^c &= -\widehat{N}_{xx}^c \frac{\partial w_0^c}{\partial x} \delta\left(\frac{\partial w_0^c}{\partial x}\right) - \widehat{N}_{yy}^c \frac{\partial w_0^c}{\partial y} \delta\left(\frac{\partial w_0^c}{\partial y}\right) - \widehat{N}_{xy}^c \frac{\partial w_0^c}{\partial x} \delta\left(\frac{\partial w_0^c}{\partial y}\right) - \widehat{N}_{xy}^c \frac{\partial w_0^c}{\partial y} \delta\left(\frac{\partial w_0^c}{\partial x}\right)
\end{aligned} \tag{25}$$

The prebuckling stresses $(\widehat{N}_{xx}^{t,b,c}, \widehat{N}_{yy}^{t,b,c}, \widehat{N}_{xy}^{t,b,c})$ depends on the in-plane loading and boundary conditions, which will be determined in next section.

The Rayleigh-Ritz approach is applied to derive the governing equations for the instability problem of VAT sandwich plates. Because the analytical formulation is derived from a weak-form energy formula, only essential boundary conditions need to be satisfied. As such, the boundary constraints in terms of the in-plane displacements ($u_0^{t,b,c}$ and $v_0^{t,b,c}$), out-of-plane placements ($w_0^{t,b,c}$) and rotations ($\phi_{x0}^{t,b,c}$ and $\phi_{y0}^{t,b,c}$) will be imposed on the four edges of VAT sandwich plate. The different boundary conditions considered in the present work are described as follows (Herein, S, C and F are denoted as simply supported, clamped and free boundary condition, respectively.):

SSSS boundary conditions:

$$\begin{aligned}
v_0^{t,b,c}(-a/2, y) = 0; \quad v_0^{t,b,c}(a/2, y) = 0; \quad u_0^{t,b,c}(x, -b/2) = 0; \quad u_0^{t,b,c}(x, b/2) = 0; \\
w_0^{t,b,c}(-a/2, y) = 0; \quad w_0^{t,b,c}(a/2, y) = 0; \quad w_0^{t,b,c}(x, -b/2) = 0; \quad w_0^{t,b,c}(x, b/2) = 0; \\
\phi_{y0}^{t,b,c}(-a/2, y) = 0; \quad \phi_{y0}^{t,b,c}(a/2, y) = 0 \quad \phi_{x0}^{t,b,c}(x, -b/2) = 0; \quad \phi_{x0}^{t,b,c}(x, b/2) = 0.
\end{aligned} \tag{26}$$

CCCC boundary condition:

$$\begin{aligned}
u_0^{t,b,c}(-a/2, y) = 0; \quad u_0^{t,b,c}(a/2, y) = 0; \quad u_0^{t,b,c}(x, -b/2) = 0; \quad u_0^{t,b,c}(x, b/2) = 0; \\
v_0^{t,b,c}(-a/2, y) = 0; \quad v_0^{t,b,c}(a/2, y) = 0; \quad v_0^{t,b,c}(x, -b/2) = 0; \quad v_0^{t,b,c}(x, b/2) = 0; \\
w_0^{t,b,c}(-a/2, y) = 0; \quad w_0^{t,b,c}(a/2, y) = 0; \quad w_0^{t,b,c}(x, -b/2) = 0; \quad w_0^{t,b,c}(x, b/2) = 0; \\
\phi_{x0}^{t,b,c}(-a/2, y) = 0; \quad \phi_{x0}^{t,b,c}(a/2, y) = 0; \quad \phi_{x0}^{t,b,c}(x, -b/2) = 0; \quad \phi_{x0}^{t,b,c}(x, b/2) = 0; \\
\phi_{y0}^{t,b,c}(-a/2, y) = 0; \quad \phi_{y0}^{t,b,c}(a/2, y) = 0; \quad \phi_{y0}^{t,b,c}(x, -b/2) = 0; \quad \phi_{y0}^{t,b,c}(x, b/2) = 0.
\end{aligned} \tag{27}$$

SFSF boundary condition:

$$\begin{aligned}
v_0^{t,b,c}(-a/2, y) = 0; \quad v_0^{t,b,c}(a/2, y) = 0; \\
w_0^{t,b,c}(-a/2, y) = 0; \quad w_0^{t,b,c}(a/2, y) = 0; \\
\phi_{y0}^{t,b,c}(-a/2, y) = 0; \quad \phi_{y0}^{t,b,c}(a/2, y) = 0.
\end{aligned} \tag{28}$$

CFCF boundary condition:

$$\begin{aligned}
u_0^{t,b,c}(-a/2, y) = 0; \quad u_0^{t,b,c}(a/2, y) = 0; \\
v_0^{t,b,c}(-a/2, y) = 0; \quad v_0^{t,b,c}(a/2, y) = 0; \\
w_0^{t,b,c}(-a/2, y) = 0; \quad w_0^{t,b,c}(a/2, y) = 0; \\
\phi_{x0}^{t,b,c}(-a/2, y) = 0; \quad \phi_{x0}^{t,b,c}(a/2, y) = 0; \\
\phi_{y0}^{t,b,c}(-a/2, y) = 0; \quad \phi_{y0}^{t,b,c}(a/2, y) = 0.
\end{aligned} \tag{29}$$

It is noted that for each case, the boundary conditions imposed on the two facesheets and the core of the sandwich plate are similar to each other in buckling regime. Furthermore, due to the fact that the Legendre polynomials are suitable for the cases with strong flexural anisotropy [55, 42], the in-plane displacements $(u_0^{t,b,c}, v_0^{t,b,c})$, out-of-plane displacements $(w_0^{t,b,c})$ and rotations $(\phi_{x0}^{t,b,c}, \phi_{y0}^{t,b,c})$ used for global buckling and wrinkling analysis are therefore constructed by Legendre polynomials multiplying with boundary functions that satisfy essential boundary conditions on four edges of the sandwich plate, for instance, the displacement fields of VAT sandwich plates are expressed as,

$$u_0^{t,b,c}(\xi, \eta) = \Psi_1(\xi, \eta) \sum_{m=0}^{M_1} \sum_{n=0}^{N_1} \mathcal{A}_{mn}^{t,b,c} L_m(\xi) L_n(\eta) \tag{30a}$$

$$v_0^{t,b,c}(\xi, \eta) = \Psi_2(\xi, \eta) \sum_{m=0}^{M_2} \sum_{n=0}^{N_2} \mathcal{B}_{mn}^{t,b,c} L_m(\xi) L_n(\eta) \tag{30b}$$

$$w_0^{t,b,c}(\xi, \eta) = \Psi_3(\xi, \eta) \sum_{m=0}^{M_3} \sum_{n=0}^{N_3} \mathcal{C}_{mn}^{t,b,c} L_m(\xi) L_n(\eta) \tag{30c}$$

$$\phi_{x0}^{t,b,c}(\xi, \eta) = \Psi_4(\xi, \eta) \sum_{m=0}^{M_4} \sum_{n=0}^{N_4} \mathcal{D}_{mn}^{t,b,c} L_m(\xi) L_n(\eta) \quad (30d)$$

$$\phi_{y0}^{t,b,c}(\xi, \eta) = \Psi_5(\xi, \eta) \sum_{m=0}^{M_5} \sum_{n=0}^{N_5} \mathcal{E}_{mn}^{t,b,c} L_m(\xi) L_n(\eta) \quad (30e)$$

with

$$\begin{aligned} \Psi_1(\xi, \eta) &= (1 + \xi)^{\psi_{11}} (1 - \xi)^{\psi_{12}} (1 + \eta)^{\psi_{13}} (1 - \eta)^{\psi_{14}} \\ \Psi_2(\xi, \eta) &= (1 + \xi)^{\psi_{21}} (1 - \xi)^{\psi_{22}} (1 + \eta)^{\psi_{23}} (1 - \eta)^{\psi_{24}} \\ \Psi_3(\xi, \eta) &= (1 + \xi)^{\psi_{31}} (1 - \xi)^{\psi_{32}} (1 + \eta)^{\psi_{33}} (1 - \eta)^{\psi_{34}} \\ \Psi_4(\xi, \eta) &= (1 + \xi)^{\psi_{41}} (1 - \xi)^{\psi_{42}} (1 + \eta)^{\psi_{43}} (1 - \eta)^{\psi_{44}} \\ \Psi_5(\xi, \eta) &= (1 + \xi)^{\psi_{51}} (1 - \xi)^{\psi_{52}} (1 + \eta)^{\psi_{53}} (1 - \eta)^{\psi_{54}} \end{aligned} \quad (31)$$

where $\xi = 2x/a$ and $\eta = 2y/b$; $L_m(\xi)$ and $L_n(\eta)$ are the m^{th} and n^{th} Legendre polynomials with respect to ξ and η , respectively; $\mathcal{A}_{mn}^{t,b,c}$, $\mathcal{B}_{mn}^{t,b,c}$, $\mathcal{C}_{mn}^{t,b,c}$, $\mathcal{D}_{mn}^{t,b,c}$ and $\mathcal{E}_{mn}^{t,b,c}$ are the corresponding polynomial coefficients of the displacement component $u_0^{t,b,c}$, $v_0^{t,b,c}$, $w_0^{t,b,c}$, $\phi_{x0}^{t,b,c}$ and $\phi_{y0}^{t,b,c}$, respectively; Ψ_1 , Ψ_2 , Ψ_3 , Ψ_4 and Ψ_5 are the functions which satisfy the essential boundary conditions along the four edges of sandwich plates; ψ_{ij} ($i = 1, 2, 3, 4, 5$; $j = 1, 2, 3, 4$) are the boundary state coefficients of the displacement component $u_0^{t,b,c}$, $v_0^{t,b,c}$, $w_0^{t,b,c}$, $\phi_{x0}^{t,b,c}$ and $\phi_{y0}^{t,b,c}$, respectively, which are given as follows:

SSSS boundary condition:

$$\begin{cases} \psi_{11} = 0; & \psi_{12} = 0; & \psi_{13} = 1; & \psi_{14} = 1; \\ \psi_{21} = 1; & \psi_{22} = 1; & \psi_{23} = 0; & \psi_{24} = 0; \\ \psi_{31} = 1; & \psi_{32} = 1; & \psi_{33} = 1; & \psi_{34} = 1; \\ \psi_{41} = 0; & \psi_{42} = 0; & \psi_{43} = 1; & \psi_{44} = 1; \\ \psi_{51} = 1; & \psi_{52} = 1; & \psi_{53} = 0; & \psi_{54} = 0. \end{cases} \quad (32)$$

CCCC boundary condition:

$$\begin{cases} \psi_{11} = 1; & \psi_{12} = 1; & \psi_{13} = 1; & \psi_{14} = 1; \\ \psi_{21} = 1; & \psi_{22} = 1; & \psi_{23} = 1; & \psi_{24} = 1; \\ \psi_{31} = 1; & \psi_{32} = 1; & \psi_{33} = 1; & \psi_{34} = 1; \\ \psi_{41} = 1; & \psi_{42} = 1; & \psi_{43} = 1; & \psi_{44} = 1; \\ \psi_{51} = 1; & \psi_{52} = 1; & \psi_{53} = 1; & \psi_{54} = 1. \end{cases} \quad (33)$$

SFSF boundary condition:

$$\begin{cases} \psi_{11} = 0; & \psi_{12} = 0; & \psi_{13} = 0; & \psi_{14} = 0; \\ \psi_{21} = 1; & \psi_{22} = 1; & \psi_{23} = 0; & \psi_{24} = 0; \\ \psi_{31} = 1; & \psi_{32} = 1; & \psi_{33} = 0; & \psi_{34} = 0; \\ \psi_{41} = 0; & \psi_{42} = 0; & \psi_{43} = 0; & \psi_{44} = 0; \\ \psi_{51} = 1; & \psi_{52} = 1; & \psi_{53} = 0; & \psi_{54} = 0. \end{cases} \quad (34)$$

CFCF boundary condition:

$$\begin{cases} \psi_{11} = 1; & \psi_{12} = 1; & \psi_{13} = 0; & \psi_{14} = 0; \\ \psi_{21} = 1; & \psi_{22} = 1; & \psi_{23} = 0; & \psi_{24} = 0; \\ \psi_{31} = 1; & \psi_{32} = 1; & \psi_{33} = 0; & \psi_{34} = 0; \\ \psi_{41} = 1; & \psi_{42} = 1; & \psi_{43} = 0; & \psi_{44} = 0; \\ \psi_{51} = 1; & \psi_{52} = 1; & \psi_{53} = 0; & \psi_{54} = 0; \end{cases} \quad (35)$$

Substituting Eqs. (30) into the strain-displacement equations, Eqs. (10), (11) and (13), and the constitutive equations, Eqs. (16) and (23), and then into Eqs. (21) and (24), applying the principle of minimum potential energy Eq. (18) and minimizing with respect to the unknown coefficients $\mathcal{A}_{mn}^{t,b,c}$ ($m = 0, 1, \dots, M_1; n = 0, 1, \dots, N_1$), $\mathcal{B}_{mn}^{t,b,c}$ ($m = 0, 1, \dots, M_2; n = 0, 1, \dots, N_2$), $\mathcal{C}_{mn}^{t,b,c}$ ($m = 0, 1, \dots, M_3; n = 0, 1, \dots, N_3$), $\mathcal{D}_{mn}^{t,b,c}$ ($m = 0, 1, \dots, M_4; n = 0, 1, \dots, N_4$) and $\mathcal{E}_{mn}^{t,b,c}$ ($m = 0, 1, \dots, M_5; n = 0, 1, \dots, N_5$), a set

of algebraic equations is then obtained and expressed in the following matrix form:

$$\left(\begin{array}{c} \left[\begin{array}{ccccc} \mathbf{K}_{11} & \mathbf{K}_{12} & \mathbf{K}_{13} & \mathbf{K}_{14} & \mathbf{K}_{15} \\ \mathbf{K}_{12} & \mathbf{K}_{22} & \mathbf{K}_{23} & \mathbf{K}_{24} & \mathbf{K}_{25} \\ \mathbf{K}_{13} & \mathbf{K}_{23} & \mathbf{K}_{33} & \mathbf{K}_{34} & \mathbf{K}_{35} \\ \mathbf{K}_{14} & \mathbf{K}_{24} & \mathbf{K}_{34} & \mathbf{K}_{44} & \mathbf{K}_{45} \\ \mathbf{K}_{15} & \mathbf{K}_{25} & \mathbf{K}_{35} & \mathbf{K}_{45} & \mathbf{K}_{55} \end{array} \right] + \lambda \left[\begin{array}{ccccc} 0 & 0 & 0 & 0 & 0 \\ 0 & 0 & 0 & 0 & 0 \\ 0 & 0 & \mathbf{L}_{33} & 0 & 0 \\ 0 & 0 & 0 & 0 & 0 \\ 0 & 0 & 0 & 0 & 0 \end{array} \right] \end{array} \right) \left\{ \begin{array}{c} \mathcal{A} \\ \mathcal{B} \\ \mathcal{C} \\ \mathcal{D} \\ \mathcal{E} \end{array} \right\} = \left\{ \begin{array}{c} 0 \\ 0 \\ 0 \\ 0 \\ 0 \end{array} \right\} \quad (36)$$

where \mathbf{K}_{ij} ($i, j = 1, 2, 3, 4, 5$) is the stiffness matrix of the VAT composite sandwich plate. The symbols 1, 2, 3, 4, and 5 in the subscript of each stiffness matrix corresponding to the in-plane displacement $u_0^{t,b,c}$, the in-plane displacement $v_0^{t,b,c}$, the out-plane displacement $w_0^{t,b,c}$, the rotation $\phi_{x0}^{t,b,c}$ around the x -axis, and the rotation $\phi_{y0}^{t,b,c}$ around the y -axis, respectively, and in particular, a combination of two different symbols represents the coupling effect between them. Note, each stiffness matrix in Eq. (36) contains the contributions from both the two facesheets and the core. In addition, \mathbf{L}_{33} denotes the geometric stiffness matrix obtained from the virtual work done by the prebuckling stresses, for instance, Eq. (25); λ is the eigenvalue; $\{\mathcal{A}, \mathcal{B}, \mathcal{C}, \mathcal{D}, \mathcal{E}\}^T$ is the vector of unknown coefficients corresponding to the shape functions, which includes the contribution from both the two facesheet and the core. The buckling loads and the corresponding instability patterns of VAT sandwich plates can be obtained by solving the eigenvalue problem defined in Eq. (36). A numerical routine based on Eq. (36) was implemented in MATLAB for both global buckling and wrinkling analysis of VAT sandwich plates under in-plane compressive loads.

4. Prebuckling analysis

Before the prebuckling analysis, three major assumptions are made as follows: (1) Both the top and bottom facesheets are the same with each other in terms of material properties, geometric properties and layup configurations. Considering that the core is of a fully three-dimensional, orthotropic solid body, the entire sandwich plate is therefore symmetrical with respect to its own mid-plane. (2) The core is assumed to be perfectly bonded with both top and bottom facesheets during the prebuckling regime, and thus the compatibility conditions at the face-core interfaces of sandwich plates are fully satisfied. (3) The normal stress (σ_{zz}^c) along the thickness direction of the core induced by the Poisson effect is

negligible. Therefore, the sandwich plate is in a plane stress state during the prebuckling regime, and the equivalent single layer theory can be applied to determine the prebuckling stress distribution for both the two facesheets and the core of VAT sandwich plates. Herein, the Rayleigh-Ritz formulation based on the principle of minimum complementary energy is adopted to solve the prebuckling problem of VAT sandwich plates with general in-plane boundary constraint. As the entire sandwich plate is symmetrical with respect to its mid-plane, the relationship between the in-plane and out-of-plane behaviours within the sandwich plate is uncoupled. The in-plane strains (ε_{xx}^0 , ε_{yy}^0 , and γ_{xy}^0) are expressed in terms of the in-plane stress resultants (N_{xx}^0 , N_{yy}^0 , and N_{xy}^0) in the ESL theory framework as follows [54, 51],

$$\begin{Bmatrix} \varepsilon_{xx}^0 \\ \varepsilon_{yy}^0 \\ \gamma_{xy}^0 \end{Bmatrix} = \begin{bmatrix} a_{11}^0(x, y) & a_{12}^0(x, y) & a_{16}^0(x, y) \\ a_{12}^0(x, y) & a_{22}^0(x, y) & a_{26}^0(x, y) \\ a_{16}^0(x, y) & a_{26}^0(x, y) & a_{66}^0(x, y) \end{bmatrix} \begin{Bmatrix} N_{xx}^0 \\ N_{yy}^0 \\ N_{xy}^0 \end{Bmatrix} \quad (37)$$

where the superscript 0 that is distinguished from the superscripts t (top facesheet), b (bottom facesheet) and c (core) represents the entire sandwich plate under the ESL theory framework, unless otherwise specified. a_{ij}^0 ($i, j = 1, 2, 6$) are the in-plane compliance coefficients, which can be obtained from

$$\begin{bmatrix} a_{11}^0(x, y) & a_{12}^0(x, y) & a_{16}^0(x, y) \\ a_{12}^0(x, y) & a_{22}^0(x, y) & a_{26}^0(x, y) \\ a_{16}^0(x, y) & a_{26}^0(x, y) & a_{66}^0(x, y) \end{bmatrix} = \begin{bmatrix} A_{11}^0(x, y) & A_{12}^0(x, y) & A_{16}^0(x, y) \\ A_{12}^0(x, y) & A_{22}^0(x, y) & A_{26}^0(x, y) \\ A_{16}^0(x, y) & A_{26}^0(x, y) & A_{66}^0(x, y) \end{bmatrix}^{-1} \quad (38)$$

Herein, the core within the sandwich plate can be regarded as a composite lamina with the principal material direction of orthotropy oriented at an angle of 0° with respect to the x -axis. The in-plane stress resultants (N_{xx}^0 , N_{yy}^0 and N_{xy}^0) are represented by the Airy's stress function Φ as,

$$N_{xx}^0 = \frac{\partial^2 \Phi}{\partial y^2}, \quad N_{yy}^0 = \frac{\partial^2 \Phi}{\partial x^2}, \quad N_{xy}^0 = -\frac{\partial^2 \Phi}{\partial x \partial y} \quad (39)$$

Furthermore, the complementary energy of the VAT composite sandwich plates without considering any in-plane boundary conditions is expressed in terms of the Airy's stress

function Φ as,

$$\begin{aligned} \Pi_C = \frac{1}{2} \iint_{\Omega} \left\{ a_{11}^0 \left(\frac{\partial^2 \Phi}{\partial y^2} \right)^2 + 2a_{12}^0 \frac{\partial^2 \Phi}{\partial x^2} \frac{\partial^2 \Phi}{\partial y^2} + a_{22}^0 \left(\frac{\partial^2 \Phi}{\partial x^2} \right)^2 - 2a_{16}^0 \frac{\partial^2 \Phi}{\partial y^2} \frac{\partial^2 \Phi}{\partial x \partial y} \right. \\ \left. - 2a_{26}^0 \frac{\partial^2 \Phi}{\partial x^2} \frac{\partial^2 \Phi}{\partial x \partial y} + a_{66}^0 \left(\frac{\partial^2 \Phi}{\partial x \partial y} \right)^2 \right\} dx dy \end{aligned} \quad (40)$$

In the following, the Rayleigh-Ritz formulation combined with the Lagrange multiplier method is applied to determine the prebuckling stresses for both facesheets and core of the VAT sandwich plates. The proposed approach for solving the prebuckling problem of the sandwich plate is general in terms of in-plane boundary conditions and loading cases [51]. Note, the VAT sandwich plates under uniform end-shortening, which leads to mixed stress and displacement boundary conditions, is only studied in this paper. For the sake of completeness, however, three different types of in-plane boundary conditions are briefly introduced herein, i.e., pure stress boundary condition (Case-A), pure displacement boundary condition (Case-B) and mixed stress and displacement boundary condition (Case-C). The Case-C boundary condition is mainly considered in this paper.

Case-A

If only pure stress in-plane boundary conditions are considered, the Airy's stress function Φ is constructed by employing the semi-inverse method, i.e., the admissible functions can be directly chosen to satisfy the natural (or force) boundary conditions along the four edges of the plate, as follows, [44]

$$\Phi(\xi, \eta) = \Phi_0(\xi, \eta) + (1 - \xi^2)^2(1 - \eta^2)^2 \sum_{p=0}^P \sum_{q=0}^Q \mathcal{G}_{pq} L_p(\xi) L_q(\eta) \quad (41)$$

where $\xi = 2x/a$ and $\eta = 2y/b$; $L_p(\xi)$ and $L_q(\eta)$ are the p^{th} and q^{th} Legendre polynomials with respect to ξ and η , respectively. Φ_0 satisfies the applied stress constraint condition along the edges of the plate, while the second part on the right hand side of Eq. (41) satisfies the stress-free boundary conditions. Applying the semi-inverse method to construct the Airy's stress function Φ depends on the characteristics of both layup configuration and in-plane boundary constraint. Nevertheless, there always remains a challenging for the traditional semi-inverse modelling method to deal with complex in-plane boundary constraints such as non-uniform shear boundary constraint. Recently, Wu et al. [56] and

Chen and Nie [51] proposed an generalised Rayleigh-Ritz approach combined with the Lagrange multiplier method, which has been successfully used for predicting the in-plane response of VAT composite plates with general boundary constraints [51, 52]. By means of applying the Lagrange multiplier method, the individual admissible function do not need to satisfy the natural (or force) boundary conditions, alternatively, the series function as a whole is imposed to satisfy the boundary conditions by introducing additional constraint equations. In so doing, the requirement of satisfying the boundary conditions for the admissible functions in the Rayleigh-Ritz method is relaxed, and it is more appropriate to deal with general in-plane boundary conditions. Based on this modelling strategy, the Airy's stress function Φ is directly expressed as,

$$\Phi(\xi, \eta) = \sum_{p=0}^P \sum_{q=0}^Q \mathcal{G}_{pq} L_p(\xi) L_q(\eta) \quad (42)$$

Substituting Eq. (42) into Eq. (39), the in-plane stress resultants (N_{xx}^0 , N_{yy}^0 and N_{xy}^0) are expanded as,

$$\begin{aligned} N_{xx}^0 &= \frac{4}{b^2} \sum_{p=0}^P \sum_{q=2}^Q \mathcal{G}_{pq} L_p(\xi) \frac{\partial^2 L_q(\eta)}{\partial \eta^2} \\ N_{yy}^0 &= \frac{4}{a^2} \sum_{p=2}^P \sum_{q=0}^Q \mathcal{G}_{pq} \frac{\partial^2 L_p(\xi)}{\partial \xi^2} L_q(\eta) \\ -N_{xy}^0 &= \frac{4}{ab} \sum_{p=1}^P \sum_{q=1}^Q \mathcal{G}_{pq} \frac{\partial L_p(\xi)}{\partial \xi} \frac{\partial L_q(\eta)}{\partial \eta} \end{aligned} \quad (43)$$

If the boundary stress distribution (\tilde{N}_{xx}^0 , \tilde{N}_{yy}^0 , and \tilde{N}_{xy}^0) along the four edges of the sandwich plate is prescribed, the following expressions can be obtained by using Eq. (43):

$$\begin{aligned} \tilde{N}_{xx}^0(\eta) \Big|_{\xi=-1} &= \frac{4}{b^2} \sum_{q=2}^Q \Lambda_q^1 \frac{\partial^2 L_q(\eta)}{\partial \eta^2}, & \tilde{N}_{xx}^0(\eta) \Big|_{\xi=1} &= \frac{4}{b^2} \sum_{q=2}^Q \Lambda_q^2 \frac{\partial^2 L_q(\eta)}{\partial \eta^2} \\ \tilde{N}_{yy}^0(\xi) \Big|_{\eta=-1} &= \frac{4}{a^2} \sum_{p=2}^P \Lambda_p^3 \frac{\partial^2 L_p(\xi)}{\partial \xi^2}, & \tilde{N}_{yy}^0(\xi) \Big|_{\eta=1} &= \frac{4}{a^2} \sum_{p=2}^P \Lambda_p^4 \frac{\partial^2 L_p(\xi)}{\partial \xi^2} \\ \tilde{N}_{xy}^0(\eta) \Big|_{\xi=-1} &= -\frac{4}{ab} \sum_{q=1}^Q \Lambda_q^5 \frac{\partial L_q(\eta)}{\partial \eta}, & \tilde{N}_{xy}^0(\eta) \Big|_{\xi=1} &= -\frac{4}{ab} \sum_{q=1}^Q \Lambda_q^6 \frac{\partial L_q(\eta)}{\partial \eta} \\ \tilde{N}_{xy}^0(\xi) \Big|_{\eta=-1} &= -\frac{4}{ab} \sum_{p=1}^P \Lambda_p^7 \frac{\partial L_p(\xi)}{\partial \xi}, & \tilde{N}_{xy}^0(\xi) \Big|_{\eta=1} &= -\frac{4}{ab} \sum_{p=1}^P \Lambda_p^8 \frac{\partial L_p(\xi)}{\partial \xi} \end{aligned} \quad (44)$$

with

$$\begin{aligned}
\Lambda_q^1 &= \sum_{p=0}^P \mathcal{G}_{pq} L_p(-1), & \Lambda_q^2 &= \sum_{p=0}^P \mathcal{G}_{pq} L_p(1) \\
\Lambda_p^3 &= \sum_{q=0}^Q \mathcal{G}_{pq} L_q(-1), & \Lambda_p^4 &= \sum_{q=0}^Q \mathcal{G}_{pq} L_q(1) \\
\Lambda_q^5 &= \sum_{p=1}^P \mathcal{G}_{pq} \frac{\partial L_p(\xi)}{\partial \xi} \Big|_{\xi=-1}, & \Lambda_q^6 &= \sum_{p=1}^P \mathcal{G}_{pq} \frac{\partial L_p(\xi)}{\partial \xi} \Big|_{\xi=1} \\
\Lambda_p^7 &= \sum_{q=1}^Q \mathcal{G}_{pq} \frac{\partial L_q(\eta)}{\partial \eta} \Big|_{\eta=-1}, & \Lambda_p^8 &= \sum_{q=1}^Q \mathcal{G}_{pq} \frac{\partial L_q(\eta)}{\partial \eta} \Big|_{\eta=1}
\end{aligned} \tag{45}$$

where Λ_j^i ($i = 1, 2, \dots, 8$; $j = p, q$) is the j^{th} boundary stress coefficient on the i^{th} stress boundary condition, which can be determined by applying the appropriate mathematical curve fitting method to Eq. (44). In the present work, a linear fitting method combined with a set of control points is adopted to retrieve the boundary stress coefficients from the in-plane stress boundary conditions given by Eq. (44). The Chebyshev–Gauss–Labotto point distribution, due to its non-uniformity and stability, is superior to the uniform point distribution in capturing the local feature of the boundary stress distribution and is thus chosen to be distributed on the boundary edges ($\xi = \pm 1, \eta = \pm 1$) of the plate, which are given as

$$\begin{aligned}
\xi = \pm 1 : \quad \eta_j &= \cos\left(\frac{j-1}{\mathcal{N}_{CGL}^\eta - 1} \pi\right) \quad j = 1, 2, \dots, \mathcal{N}_{CGL}^\eta \\
\eta = \pm 1 : \quad \xi_i &= \cos\left(\frac{i-1}{\mathcal{N}_{CGL}^\xi - 1} \pi\right) \quad i = 1, 2, \dots, \mathcal{N}_{CGL}^\xi
\end{aligned} \tag{46}$$

where \mathcal{N}_{CGL}^η and \mathcal{N}_{CGL}^ξ are the number of the Chebyshev–Gauss–Labotto points, which equals to the number of terms in each stress boundary condition of Eq. (44). Substituting the Chebyshev–Gauss–Labotto points into Eq. (44), a set of linear algebraic equations corresponding to each stress boundary condition can be obtained. A detailed process of determining the boundary stress coefficients can be found in Ref. [51]. Furthermore, the constraint equations in Eq. (45) need to be included into the complementary energy Π_C to build a Lagrange function \mathbb{L}_A , that is,

$$\mathbb{L}_A(\mathcal{G}_{00}, \mathcal{G}_{01}, \dots, \mathcal{G}_{PQ}, \chi_2^1, \chi_3^1, \dots, \chi_P^8) = \Pi_C + \Pi_{LM}^* \tag{47}$$

with

$$\begin{aligned}
\Pi_{\text{LM}}^* = & \frac{4}{b^2} \sum_{q=2}^Q \chi_q^1 \left(\sum_{p=0}^P \mathcal{G}_{pq} L_p(-1) - \Lambda_q^1 \right) + \frac{4}{b^2} \sum_{q=2}^Q \chi_q^2 \left(\sum_{p=0}^P \mathcal{G}_{pq} L_p(1) - \Lambda_q^2 \right) + \\
& \frac{4}{a^2} \sum_{p=2}^P \chi_p^3 \left(\sum_{q=0}^Q \mathcal{G}_{pq} L_q - \Lambda_p^3 \right) + \frac{4}{a^2} \left(\sum_{p=2}^P \chi_p^4 \sum_{q=0}^Q \mathcal{G}_{pq} L_q(1) - \Lambda_p^4 \right) - \\
& \frac{4}{ab} \sum_{q=1}^Q \chi_q^5 \left(\sum_{p=1}^P \mathcal{G}_{pq} \frac{\partial L_p(\xi)}{\partial \xi} \Big|_{\xi=-1} - \Lambda_q^5 \right) - \frac{4}{ab} \sum_{q=1}^Q \chi_q^6 \left(\sum_{p=1}^P \mathcal{G}_{pq} \frac{\partial L_p(\xi)}{\partial \xi} \Big|_{\xi=1} - \Lambda_q^6 \right) - \\
& \frac{4}{ab} \sum_{p=1}^P \chi_p^7 \left(\sum_{q=1}^Q \mathcal{G}_{pq} \frac{\partial L_q(\eta)}{\partial \eta} \Big|_{\eta=-1} - \Lambda_p^7 \right) - \frac{4}{ab} \sum_{p=1}^P \chi_p^8 \left(\sum_{q=1}^Q \mathcal{G}_{pq} \frac{\partial L_q(\eta)}{\partial \eta} \Big|_{\eta=1} - \Lambda_p^8 \right)
\end{aligned} \tag{48}$$

where χ_j^i ($i = 1, 2, \dots, 8; j = p, q$) are the j^{th} Lagrange multiplier on the i^{th} stress boundary condition; Π_{LM}^* represents the constraint function generated by the stress boundary conditions on four edges of the sandwich plate. Substituting Eq. (43) into Eqs. (40) and (47), and minimizing the Lagrange function $\mathbb{L}_{\mathbb{A}}$ with respect to \mathcal{G}_{pq} ($p = 0, 1, \dots, P; q = 0, 1, \dots, Q$) and χ_j^i ($i = 1, 2, \dots, 8; j = p, q$), that is,

$$\frac{\partial \mathbb{L}_{\mathbb{A}}}{\partial \mathcal{G}_{pq}} = 0, \quad \frac{\partial \mathbb{L}_{\mathbb{A}}}{\partial \chi_j^i} = 0 \tag{49}$$

a set of linear algebraic equations can be obtained and expressed in the following matrix form:

$$\begin{bmatrix} \mathbf{K} & \mathbf{LM} \\ \mathbf{LM}^{\text{T}} & \mathbf{0} \end{bmatrix} \begin{Bmatrix} \mathcal{G} \\ \chi \end{Bmatrix} = \begin{Bmatrix} \mathbf{0} \\ \mathbf{\Lambda} \end{Bmatrix} \tag{50}$$

where \mathbf{K} is the extensional stiffness matrix of the sandwich plate; \mathbf{LM} is the Lagrange multiplier matrix generated by the constraint conditions; \mathbf{LM}^{T} is the transposed form of \mathbf{LM} ; \mathcal{G} and χ are the unknown vectors to be determined; $\mathbf{\Lambda}$ is the boundary stress vector, which is related to the prescribed stress distribution on the edges of the sandwich plate.

Case B

Without loss of generality, the in-plane displacement boundary conditions on four edges ($\xi = \pm 1, \eta = \pm 1$) of the sandwich plate can be expressed as

$$\begin{aligned} \xi = -1 : \begin{cases} u^0 = \tilde{u}_1^0(\eta) \\ v^0 = \tilde{v}_1^0(\eta) \end{cases} ; \quad \xi = 1 : \begin{cases} u^0 = \tilde{u}_2^0(\eta) \\ v^0 = \tilde{v}_2^0(\eta) \end{cases} \\ \eta = -1 : \begin{cases} u^0 = \tilde{u}_3^0(\xi) \\ v^0 = \tilde{v}_3^0(\xi) \end{cases} ; \quad \eta = 1 : \begin{cases} u^0 = \tilde{u}_4^0(\xi) \\ v^0 = \tilde{v}_4^0(\xi) \end{cases} \end{aligned} \quad (51)$$

where \tilde{u}_i^0 and \tilde{v}_i^0 ($i = 1, 2, 3, 4$) are the prescribed in-plane displacements on the i^{th} boundary edge of the sandwich plate. As the boundary conditions on four edges are specified solely in terms of displacements, there exists no stress boundary constraints along the edges of the sandwich plate. As such, the stress constraint function Π_{LM}^* obtained by applying the Lagrange multiplier method is unnecessary. However, the displacement boundary constraints on four edges of the plate require to be satisfied in boundary integral form and given by [51]

$$\begin{aligned} \Pi_{\text{D}}^* = & \frac{2}{b} \int_{-1}^1 \left[\frac{\partial^2 \Phi}{\partial \eta^2} \tilde{u}_1^0 \right]_{\xi=-1} d\eta - \frac{2}{a} \int_{-1}^1 \left[\frac{\partial^2 \Phi}{\partial \xi \partial \eta} \tilde{v}_1^0 \right]_{\xi=-1} d\eta + \\ & \frac{2}{b} \int_{-1}^1 \left[\frac{\partial^2 \Phi}{\partial \eta^2} \tilde{u}_2^0 \right]_{\xi=1} d\eta - \frac{2}{a} \int_{-1}^1 \left[\frac{\partial^2 \Phi}{\partial \xi \partial \eta} \tilde{v}_2^0 \right]_{\xi=1} d\eta - \\ & \frac{2}{b} \int_{-1}^1 \left[\frac{\partial^2 \Phi}{\partial \xi \partial \eta} \tilde{u}_3^0 \right]_{\eta=-1} d\xi + \frac{2}{a} \int_{-1}^1 \left[\frac{\partial^2 \Phi}{\partial \xi^2} \tilde{v}_3^0 \right]_{\eta=-1} d\xi - \\ & \frac{2}{b} \int_{-1}^1 \left[\frac{\partial^2 \Phi}{\partial \xi \partial \eta} \tilde{u}_4^0 \right]_{\eta=1} d\xi + \frac{2}{a} \int_{-1}^1 \left[\frac{\partial^2 \Phi}{\partial \xi^2} \tilde{v}_4^0 \right]_{\eta=1} d\xi \end{aligned} \quad (52)$$

where Π_{D}^* denotes the displacement constraint function representing the work done by the unknown force along the applied boundary displacement. Accordingly, imposing the in-plane displacement boundary constraint Π_{D}^* into the complementary energy Eq. (40), we can obtain

$$\Pi_{\text{Total}} = \Pi_{\text{C}} + \Pi_{\text{D}}^* \quad (53)$$

Substituting Eq. (43) into Eqs. (40) and (52) and then into Eq. (53), and minimizing the total complementary energy Π_{Total} with respect to \mathcal{G}_{pq} ($p = 0, 1, \dots, P; q = 0, 1, \dots, Q$)

as,

$$\frac{\partial \Pi_{\text{Total}}}{\partial \mathcal{G}_{pq}} = 0 \quad (54)$$

a set of linear algebraic equations is then generated and expressed in the following matrix form:

$$\mathbf{K}\mathcal{G} = \mathbf{P} \quad (55)$$

where \mathbf{K} and \mathcal{G} are similar to those in Eq. (50). \mathbf{P} is a load vector, which is related to the prescribed in-plane displacement along the edges of the sandwich plate.

Case C

For a general case, both in-plane stress and displacement boundary conditions are applied simultaneously. Therefore, both the stress constraint conditions Π_{LM}^* and displacement boundary conditions Π_{D}^* need to be imposed into the complementary energy Π_{C} to derive a Lagrange function \mathbb{L}_{A} , as follows,

$$\mathbb{L}_{\text{A}}(\mathcal{G}_{00}, \mathcal{G}_{01}, \dots, \mathcal{G}_{PQ}, \chi_2^1, \chi_3^1, \dots, \chi_P^8) = \Pi_{\text{C}} + \Pi_{\text{LM}}^* + \Pi_{\text{D}}^* \quad (56)$$

Substituting Eq. (43) into Eqs. (40), (48) and (52) and then into Eq. (56), and minimizing the Lagrange function \mathbb{L}_{A} with respect to \mathcal{G}_{pq} ($p = 0, 1, \dots, P; q = 0, 1, \dots, Q$) and χ_j^i ($i = 1, 2, \dots, 8; j = p, q$) as,

$$\frac{\partial \mathbb{L}_{\text{A}}}{\partial \mathcal{G}_{pq}} = 0, \quad \frac{\partial \mathbb{L}_{\text{A}}}{\partial \chi_j^i} = 0 \quad (57)$$

A set of linear algebraic equations governing the in-plane stress problem of composite plates subjected to mixed in-plane boundary conditions can be obtained and expressed in the following matrix form:

$$\begin{bmatrix} \mathbf{K} & \mathbf{LM} \\ \mathbf{LM}^{\text{T}} & \mathbf{O} \end{bmatrix} \begin{Bmatrix} \mathcal{G} \\ \chi \end{Bmatrix} = \begin{Bmatrix} \mathbf{P} \\ \Lambda \end{Bmatrix} \quad (58)$$

The in-plane stress and displacement boundary conditions along each boundary edge are conjugate, which indicates that if the in-plane displacement constraint condition in

that direction of the edge is activated, the conjugate stress constraint condition tends to be suppressed, and vice versa. From this point of view, there exists two extreme cases, for instance, when the stress boundary constraints are imposed on all four edges of the sandwich plate, the corresponding displacement boundary constraints are dormant and thus the terms induced by the displacement constraint function Π_D^* needs to be removed from Eq. (58), which eventually leads to Eq. (50). On the other hand, when the displacement boundary constraints are imposed on all four edges of the sandwich plate, the corresponding stress boundary constraints are suppressed and thus the stress constraint function Π_{LM}^* needs to be removed from Eq. (58), which eventually leads to Eq. (55). In the present work, however, particular attention is paid to the case of mixed in-plane boundary condition, for instance, if the sandwich plate is subjected to uniform end-shortening with transverse edges free to deform, the in-plane boundary condition is written as

$$\begin{aligned} x = \pm a/2 : \quad u^0(\pm a/2, y) = \mp \Delta_x; \quad N_{xy}^0(\pm a/2, y) = 0 \\ y = \pm b/2 : \quad N_{yy}^0(x, \pm b/2) = 0; \quad N_{yx}^0(x, \pm b/2) = 0 \end{aligned} \quad (59)$$

For this case studied, the boundary stress coefficients related to the prescribed stress boundary conditions equal to zero, that is,

$$\begin{aligned} 0 &= \sum_{q=0}^Q \mathcal{G}_{pq} L_q(-1), \quad 0 = \sum_{q=0}^Q \mathcal{G}_{pq} L_q(1) \\ 0 &= \sum_{p=1}^P \mathcal{G}_{pq} \frac{\partial L_p(\xi)}{\partial \xi} \Big|_{\xi=-1}, \quad 0 = \sum_{p=1}^P \mathcal{G}_{pq} \frac{\partial L_p(\xi)}{\partial \xi} \Big|_{\xi=1} \\ 0 &= \sum_{q=1}^Q \mathcal{G}_{pq} \frac{\partial L_q(\eta)}{\partial \eta} \Big|_{\eta=-1}, \quad 0 = \sum_{q=1}^Q \mathcal{G}_{pq} \frac{\partial L_q(\eta)}{\partial \eta} \Big|_{\eta=1} \end{aligned} \quad (60)$$

As such, the stress constraint function Π_{LM}^* can be simplified as

$$\begin{aligned} \Pi_{LM}^* &= \frac{4}{a^2} \sum_{p=2}^P \chi_p^3 \sum_{q=0}^Q \phi_{pq} L_q(-1) + \frac{4}{a^2} \sum_{p=2}^P \chi_p^4 \sum_{q=0}^Q \phi_{pq} L_q(1) \\ &\quad - \frac{4}{ab} \sum_{q=1}^Q \chi_q^5 \sum_{p=1}^P \phi_{pq} \frac{\partial L_p(\xi)}{\partial \xi} \Big|_{\xi=-1} - \frac{4}{ab} \sum_{q=1}^Q \chi_q^6 \sum_{p=1}^P \phi_{pq} \frac{\partial L_p(\xi)}{\partial \xi} \Big|_{\xi=1} \\ &\quad - \frac{4}{ab} \sum_{p=1}^P \chi_p^7 \sum_{q=1}^Q \phi_{pq} \frac{\partial L_q(\eta)}{\partial \eta} \Big|_{\eta=-1} - \frac{4}{ab} \sum_{p=1}^P \chi_p^8 \sum_{q=1}^Q \phi_{pq} \frac{\partial L_q(\eta)}{\partial \eta} \Big|_{\eta=1} \end{aligned} \quad (61)$$

At the same time, the displacement constraint function Π_D^* can be degenerated into

$$\Pi_D^* = - \int_{-1}^1 \frac{2}{b} \frac{\partial^2 \Phi}{\partial \eta^2} \Delta_x d\eta - \int_{-1}^1 \frac{2}{b} \frac{\partial^2 \Phi}{\partial \eta^2} \Delta_x d\eta \quad (62)$$

Finally, the prebuckling problem of the VAT composite sandwich plate subjected to uniform end-shortening can be solved through Eq. (58). With the aid of Eqs. (37) and (39), the prebuckling stresses ($\widehat{N}_{xx}^{t,b,c}$, $\widehat{N}_{yy}^{t,b,c}$, and $\widehat{N}_{xy}^{t,b,c}$) of both the two facesheets and the core within the VAT composite sandwich plate under uniform end-shortening can be determined from

$$\begin{Bmatrix} \widehat{N}_{xx}^{t,b,c} \\ \widehat{N}_{yy}^{t,b,c} \\ \widehat{N}_{xy}^{t,b,c} \end{Bmatrix} = \begin{bmatrix} A_{11}^{t,b,c}(x, y) & A_{12}^{t,b,c}(x, y) & A_{16}^{t,b,c}(x, y) \\ A_{12}^{t,b,c}(x, y) & A_{22}^{t,b,c}(x, y) & A_{26}^{t,b,c}(x, y) \\ A_{16}^{t,b,c}(x, y) & A_{26}^{t,b,c}(x, y) & A_{66}^{t,b,c}(x, y) \end{bmatrix} \begin{Bmatrix} \varepsilon_{xx}^0 \\ \varepsilon_{yy}^0 \\ \gamma_{xy}^0 \end{Bmatrix} \quad (63)$$

where A_{ij}^c ($i, j = 1, 2, 6$) denotes the extensional stiffness of the core. Note, in the prebuckling analysis, the contributions from both the two facesheets and the core to the overall extensional stiffness of the entire sandwich plate are taken into account. In fact, this loading condition simulates the situation of sandwich plates loaded by means of rigid blocks, where the applied in-plane load is introduced to both of the two facesheets and the core [7, 42]. Moreover, this modelling strategy for predicting the prebuckling stresses is also applicable to the case where the load is only applied to the two facesheets, while the core is unloaded. Under such circumstance, the contribution of the core to the overall extensional stiffness of the whole sandwich plate is removed from Eqs. (37) and (63). The latter loading case resembles the well-known anti-plane stress assumptions used for deriving wrinkling closed-form solutions [42].

5. Results and discussion

This section presents a detailed investigation on the instability analysis of VAT sandwich plates under in-plane compressive loads. Firstly, a series of comparison studies are conducted to validate the accuracy of the developed Rayleigh-Ritz analytical model. Subsequently, the Rayleigh-Ritz model is applied to perform several parametric studies for investigating the influences of core thickness, core orthotropy, and fibre orientation angle of the facesheets on the instability behaviours of VAT sandwich plates under uniform end-

shortening. The mechanism of applying the VAT design concept to improve the buckling resistance of sandwich plates is finally explored. In order to further validate the present Rayleigh-Ritz model, FE modelling using ABAQUS (6.12-1 version) is established for sandwich plates with relatively soft cores. The SC8R element is chosen to discretize each facesheet, whilst the C3D8R element is employed for the core's discretization. A subroutine is developed to generate the composite element with independent fibre orientations for each facesheet within the sandwich plate so that the fibre orientation angle of each ply varies according to Eq. (1). In addition, very fine meshes are used to obtain an accurate and convergent simulation for the complex response, especially in the wrinkling analysis. Note, the thickness variation of both the top and bottom facesheets within the VAT sandwich plates due to tow overlap or gaps are not considered, therefore the ply-thickness is assumed as a constant in the present work.

5.1. Comparison studies

5.1.1. Conventional sandwich plates

In order to validate the proposed Rayleigh-Ritz model for VAT sandwich plates, the global buckling problem of a short sandwich beam with orthotropic facesheets and orthotropic core given by Ji and Waas [57] is firstly studied. The sandwich beam is simply supported at both ends and subjected to a uniform end-shortening. The uniform compressive load is imposed at both the facesheets and the core, and therefore the contribution of the core to the extensional stiffness of the entire sandwich plate is considered in the prebuckling regime. The geometry of the sandwich beam is given by $a = 3\text{mm}$, $h = 1\text{mm}$, $f_t = f_b = 0.1\text{mm}$, and $2c = 0.8\text{mm}$. The material properties of the facesheets are: $E_{11}^f = 107\text{GPa}$, $E_{22}^f = E_{33}^f = 15\text{GPa}$, $G_{23}^f = G_{13}^f = G_{12}^f = 4.3\text{GPa}$, $\nu_{23}^f = \nu_{13}^f = \nu_{12}^f = 0.3$, and the material properties of the core are: $E_{33}^c = 4 \times G_{13}^c$, $G_{13}^c = G_{13}^f/200$, $\nu_{13}^c = 0.25$. The maximum number of trial functions in the loading direction is assumed to be 12, which is sufficient to accurately capture the first buckling mode. The buckling loads of the sandwich beam as a function of the orthotropy ratio E_{11}^c/E_{33}^c predicted by the present Rayleigh-Ritz model are shown in Fig. 3. The 2D exact elasticity solutions obtained by Ji and Waas [57] are also provided for the comparison purpose. Note, the buckling load P_{cr} (as used in Ref. [57]) is normalized with respect to the global beam buckling load P_B

defined as

$$P_B = \frac{P_E}{1 + P_E/\overline{GA}} \quad (64)$$

with

$$P_E = \frac{\pi^2 \overline{EI}}{a^2} \quad (65)$$

where P_E is the equivalent Euler buckling load; \overline{EI} and \overline{GA} are the effective bending stiffness and shear stiffness of the sandwich beam, respectively, which are determined according to Huang and Kardomateas [58] or Bažant et al. [59]. It is also worth highlighting that the present three-dimensional Rayleigh-Ritz model can be reduced to the two-dimensional one by eliminating the terms along the y direction such that the comparison against the results by Ji and Waas [57] is of significance in the plane-strain regime. From Fig. 3, it is clear that the normalized buckling loads obtained by the present Rayleigh-Ritz model agree well with the exact elasticity solutions given by Ji and Waas [57], even for the cases with a high orthotropy ratio E_{11}^c/E_{33}^c . The maximum error of the results shown in Fig. 3 is less than 1%. These results demonstrate the accuracy of the proposed Rayleigh-Ritz model in predicting the critical buckling load of the sandwich beam. Moreover, it is observed that the buckling mode of the sandwich beam studied herein always has only one single halfwave, which is consistent with other analysis results by Ji and Waas [57], D'Ottavio et al. [7], and Vescovini et al. [42].

The second comparison case is to study the wrinkling behaviour of a symmetrical sandwich wide beam in a general 2D plane strain state, which has been studied by Ji and Waas [60, 7, 42]. Both the boundary condition and loading condition are the same with those of the first comparison case. The geometry of the sandwich plate is defined by $a = 200\text{mm}$, $h = 70\text{mm}$, $f_t = f_b = 1\text{mm}$, and $2c = 68\text{mm}$. The material property of each facesheet is the same with that of the first comparison case, which is however replaced with the equivalent Young's modulus $E^f = 61.443\text{GPa}$ and Poisson's ratio $\nu^f = 0.0738$ [7]. The core is made of Divinycell H-grade isotropic material with Poisson's ratio $\nu^c = 0.3$ and Young's modulus E^c depends on the foam quality [61, 60, 7]: $E^c = 40\text{MPa}$ for H45 foam, $E^c = 80\text{MPa}$ for H80 foam and $E^c = 140\text{MPa}$ for H130 foam. Herein, the maximum number of trial functions in the loading direction is assumed to be 50 to ensure that a

sufficient number of buckling modes can be accurately captured. The normalized buckling strain (λ/a) as a function of the normalized half-wavelength (L_x/f_t) for sandwich beams with three different types of cores is plotted in Fig. 4 and compared against those provided by Ji and Waas [60]. Note, although the present Rayleigh-Ritz model can capture any type of wrinkling pattern (antisymmetrical or symmetrical), only the results of antisymmetric wrinkling mode, which is considered as the predominant failure mode of the sandwich wide beam in [5, 60, 7, 42], is presented herein. As shown in Fig. 4, the results obtained by the present Rayleigh-Ritz model match well with the exact elasticity solutions by Ji and Waas [60]. It was found that the buckling patterns corresponding to the lowest critical buckling strain for the sandwich wide beams with H45, H80 and H130 are the antisymmetric wrinkling modes with eight, ten, and twelve halfwaves, respectively, which are also illustrated in Fig. 4.

The third comparison case study is focused on a more complex wrinkling analysis of a three dimensional sandwich plate with each facesheet that possesses the anisotropic property. The sandwich plate is clamped on the edges of $x = \pm a/2$ and free on the edges of $y = \pm b/2$, and simultaneously loaded by a uniform end-shortening. The geometry of the sandwich plate is defined by $a = 200\text{mm}$, $b = 150\text{mm}$, $h = 52\text{mm}$, $f_t = f_b = 1\text{mm}$, and $2c = 50\text{mm}$. Each facesheet is made of four plies with stacking sequence $[\alpha/(90 + \alpha)]_s$, in which α represents the rotation of the orthotropy principal axes and varies between 0° and 90° . The material property of each facesheet is the same as that of the first comparison case, and the core is made of the isotropic material with $E_{11}^c = E_{22}^c = E_{33}^c = 20\text{MPa}$, $G_{23}^c = G_{13}^c = G_{12}^c = 13\text{MPa}$, $\nu_{23}^c = \nu_{13}^c = \nu_{12}^c = 0.25$. The maximum number of trial functions in the loading direction is assumed to be 18, which is sufficient to accurately capture the first buckling mode. The critical buckling load ($N_{x,sm}^{cr}$) predicted by the present Rayleigh-Ritz model is plotted against the rotation angle (α) in Fig. 5 and compared with those previously published by Fagerberg et al. [62] and Vescovini et al. [42]. A good agreement between the present results and those obtained in previous works is reached, which proves that the proposed Rayleigh-Ritz model is capable for the wrinkling analysis of the anisotropic sandwich plate. The wrinkling pattern of the sandwich plate for each rotation angle is of antisymmetric pattern. Furthermore, the skew angle of the wrinkles are found to vary with the rotation angle α and match well with those obtained by Fagerberg et al. [62] and Vescovini et al. [42].

In order to further demonstrate the modelling capability of present method for both global and local instability analysis of the sandwich plate, the fourth comparison case study is carried out on a rectangular sandwich plate with a large range of core thickness, as also studied by Rose et al. [63]. The sandwich plate is simply supported on four edges and loaded by a uniform end-shortening. However, the uniform compressive loading herein is only imposed on both the top and bottom facesheets, which is the same as that of Rose et al.'s work [63]. This means that the contribution of the core to the extensional stiffness of the sandwich plate is removed from the prebuckling analysis. The geometry of the sandwich plate is defined by $a = 508\text{mm}$, $b = 254\text{mm}$, $f_t = f_b = 2.794\text{mm}$ with the range of the core thickness $2c$ from 5.08mm to 203.2mm . The material properties are given for each facesheet: $E_{11}^f = E_{22}^f = E_{33}^f = 68.95\text{GPa}$, $G_{23}^f = G_{13}^f = G_{12}^f = 4.3\text{GPa}$, $\nu_{23}^f = \nu_{13}^f = \nu_{12}^f = 0.3$ and for the core: $E_{11}^c = E_{22}^c = 0.6895\text{MPa}$, $E_{33}^c = 68.95\text{MPa}$, $G_{12}^c = 0.265\text{MPa}$, $G_{13}^c = 82.74\text{MPa}$, $G_{23}^c = 49.64\text{MPa}$, $\nu_{12}^c = 0.3$, $\nu_{23}^c = \nu_{13}^c = 0.01$. The maximum number of trial functions in the loading direction is assumed to be 18, which is sufficient to accurately capture the first buckling mode. The critical buckling load ($N_{x,\text{sm}}^{\text{cr}}$) versus the normalized core thickness ($2c/a$) obtained using the present Rayleigh-Ritz model are shown in Fig. 6 and compared with those predicted by using the finite element code STAGS [63]. The results obtained using the S-GUF approach by Vescovini et al. [42] are also provided for comparison purposes. From Fig. 6, it can be seen that for a variety of core thicknesses, the present results agrees well with those published by Rose et al. [63] and Vescovini et al. [42]. Furthermore, the entire curve can be divided into two stages, that is, the buckling load of the sandwich plate gradually increases until the normalized core thickness $2c/a$ arrives at 0.06 (the first stage), and then goes down with a further increase of the normalized core thickness $2c/a$ (the second stage), accompanying by a transition from antisymmetrical buckling mode to symmetrical wrinkling mode. The buckling modes corresponding to $2c/a = 0.03$ and $2c/a = 0.2$ are also illustrated in Fig. 6. These results further demonstrate the ability of the present Rayleigh-Ritz model to accurately capture both the symmetrical and antisymmetrical buckling modes of the sandwich plate.

5.1.2. VAT sandwich plates

The fifth comparison case study is focused on the VAT sandwich plates, which are rarely studied in previous works. The current study has two major objectives: the first one

is to verify the accuracy of prebuckling stresses computation by the proposed Rayleigh-Ritz model under the assumption of membrane prebuckling state, and the second one is to analyze the both global and local instability behaviours of VAT sandwich plates. The geometry properties, material properties, and loading conditions of VAT composite sandwich plates are similar to those in the third comparison case, except that the core thickness is $2c = 10\text{mm}$ and $2c = 30\text{mm}$. Both the top and bottom facesheets are designed by the VAT design concept, and their layup configuration is $[\pm\langle 0|45\rangle]_s$. The non-uniform prebuckling stress resultants (\widehat{N}_{xx}^t , \widehat{N}_{yy}^t , and \widehat{N}_{xy}^t) of the top facesheet for the sandwich plate $[\pm\langle 0|45\rangle]_s$ with core thickness $2c = 30\text{mm}$ obtained using the present analytical formulation are presented in Fig. 7 and are found to be consistent with FEM results. The results shown in Fig. 7 approve that the proposed Rayleigh-Ritz model can accurately predict the prebuckling behaviours for VAT sandwich plates under the three assumptions outlined in Section 4. Fig. 8 shows the buckling loads and their corresponding buckling patterns for the sandwich plate $[\pm\langle 0|45\rangle]_s$ with two different core thicknesses. The results obtained by the FEM model are also included for the comparison purposes. It is obvious that the results obtained by the present Rayleigh-Ritz model agrees well with FE results for both cases of core thickness, that is, $2c = 10\text{mm}$ and $2c = 30\text{mm}$. It is also interesting that the lower core thickness ($2c = 10\text{mm}$) triggers the global instability (global buckling), while the higher core thickness ($2c = 30\text{mm}$) leads to the local instability (antisymmetrical wrinkling), which will be further studied in the parametric studies. It is noted that in order to achieve the required accuracy, a mesh density of 100×75 is selected in the $x - y$ plane of VAT sandwich plates, and one element (SC8R) for each facesheet and eight element (C3D8R) for the core were used through the depth of the sandwich plate. It took approximately 30 minutes to solve the eigenvalue problem for each sandwich plate buckling model on the computer with i7 CPU (2.9GHz) and 8G RAM.

To verify the convergence of the proposed Rayleigh-Ritz model, the critical buckling loads ($N_{x,\text{sm}}^{\text{cr}}$) of the same sandwich plate obtained using different shape-function terms in the length direction are also presented in Table 1. It is clear that the buckling loads predicted by the present Rayleigh-Ritz formulation rapidly converges to FE solutions with the increase of the number of Legendre polynomial terms. It is found that 12 terms in the length direction are sufficient to yield an accurate prediction for the buckling load of the VAT sandwich plates, and yet, despite this, 18 trial functions in the loading direction will

Table 1: Critical buckling load $N_{x,\text{sm}}^{\text{cr}}$ of the tow-steered sandwich plate $[\pm\langle 0|45\rangle]_s$ with two different core thicknesses obtained using different shape-function terms in the length direction. (unit: N/mm)

$2c$	M_i ($i = 1, 2, 3, 4, 5$)							ABAQUS
	6	8	10	12	14	16	18	
10mm	161.17	160.98	160.92	160.90	160.89	160.88	160.87	160.42
30mm	403.26	397.25	390.06	384.22	381.79	381.09	380.82	381.72

be used in the following parametric studies. It is also worth highlighting that a relatively small number of shape-function terms in the width direction is enough for both global and local instability analysis due to the fact that the sandwich plate are neither constrained nor loaded along the edges of $y = \pm b/2$. On the other hand, it was found that 9 terms of Legendre polynomial in the Airy's stress function are sufficient to obtain the convergent results in the prebuckling analysis.

5.2. Parametric studies

5.2.1. Effects of core thickness

The aim of the first parametric study is to gain a deep insight into the effect of the core thickness on the instability behaviour of VAT sandwich plates. The geometry properties, material properties, and loading conditions of the VAT sandwich plates are also similar to those in the third comparison case study except that the core thickness varies over a wide range from $2c = 2\text{mm}$ to $2c = 50\text{mm}$. The VAT layup is $[90 \pm \langle 0|75\rangle]_s$. The critical buckling load ($N_{x,\text{sm}}^{\text{cr}}$) versus the core thickness ($2c$) obtained using the present Rayleigh-Ritz formulation is shown in Fig. 9. As a relatively soft core is adopted, the results predicted using ABAQUS are also included for the comparison purpose. It is clearly seen that the core thickness has a significant influence on the instability behaviour of the VAT sandwich plates, the buckling load initially increases as the core thickness increases, and then gradually tends to be flat with the further increase of the core thickness. Furthermore, a remarkable transition of the buckling pattern from global instability (global buckling) to coupled instability and finally to local instability (wrinkling) also appears on the sandwich plate with the increase of core thickness. It is observed that either the global or coupled bucking mode remains the predominant failure mode until the core thickness $2c$ arrives at 10mm, and afterwards the wrinkling mode plays a major role in the instability process as the core thickness further increases. In particular, the effect of edge wrinkling

within the sandwich plate is pronounced when local instability occurs. The mechanism of load redistribution offered by the VAT layup $[90 \pm \langle 0|75 \rangle]_s$, which transfers a majority of compressive loads within the facesheets from the central region to both free edges, is responsible for this phenomenon of edge wrinkling. Moreover, it is also observed that the higher the core thickness, the more the halfwaves near the free edge of the facesheets, as shown in Fig. 9. In Fig. 9, the buckling mode shapes for the VAT layup $[90 \pm \langle 0|75 \rangle]_s$ with $2c = 4\text{mm}$, $2c = 10\text{mm}$, $2c = 20\text{mm}$, and $2c = 30\text{mm}$ obtained using the present Rayleigh-Ritz model are also presented. In addition, it is noted that the finite element model implemented in ABAQUS software mimics the clamped boundary conditions in an approximate manner, which results in a slight difference between the analytical results and FE solutions. However, the maximum error is found to be less than 1.7%, which means that the usage of approximate boundary condition within the FE model is appropriate and effective for both global buckling and wrinkling analysis for VAT sandwich plates with soft core.

5.2.2. Effects of core orthotropy

The second parametric study aims to investigate the effect of the core orthotropy on the buckling performance of VAT composite sandwich plates. The geometry properties of the sandwich plate are similar to those in the third comparison case study except that the thicknesses of the facesheets and the core are assumed to be $f_t = f_b = 1.0176\text{mm}$ and $2c = 30\text{mm}$, respectively. Two different boundary conditions are studied, that is, SFSF and CFCF. The entire sandwich plate is loaded by a uniform end-shortening, which means that the contribution of the core to the extensional stiffness of the sandwich plate is considered in the prebuckling analysis. The material properties are given for the highly anisotropic facesheets: $E_{11}^f = 181.0\text{GPa}$, $E_{22}^f = E_{33}^f = 10.27\text{GPa}$, $G_{23}^f = 5.96\text{GPa}$, $G_{13}^f = G_{12}^f = 7.17\text{GPa}$, $\nu_{23}^f = \nu_{13}^f = \nu_{12}^f = 0.277$ with thickness of each ply equal to 0.1272mm , and for the varying orthotropic core: $E_{11}^c = E_{22}^c = r_c E_{33}^c$, $E_{33}^c = 4 \times G_{13}^c$, $G_{23}^c = G_{13}^c = G_{12}^c = G_{13}^f/500$, $\nu_{23}^c = \nu_{13}^c = \nu_{12}^c = 0.25$, where $r_c = E_{11}^c/E_{33}^c$ represents the orthotropy ratio of the core ranging from 1 to 100. The layup configuration of both the top and bottom facesheets is chosen to be $[90 \pm \langle 0|75 \rangle]_{2s}$. The critical buckling loads ($N_{x,\text{sm}}^{\text{cr}}$) as a function of the core orthotropy ratio (E_{11}^c/E_{33}^c) for the SFSF and CFCF boundary conditions are plotted in Fig. 10 and Fig.11, respectively. The present results are also presented in Table 2 for the convenience of using as the benchmark for other nu-

Table 2: Critical buckling load $N_{x,sm}^{cf}$ of the tow-steered sandwich plate $[90 \pm (0|75)]_{2s}$ for both SFSF and CFCF boundary conditions. (unit: N/mm)

Boundary type	E_{11}^c/E_{33}^c										
	1	10	20	30	40	50	60	70	80	90	100
SFSF	260.73	296.85	329.01	357.17	378.96	397.02	408.75	410.92	412.71	414.21	415.49
CFCF	262.01	297.51	332.47	361.35	384.22	401.58	414.59	424.11	430.90	435.73	439.55

merical or analytical results. Note, the results obtained using ABAQUS are not provided herein, since that the commercial FE packages such as ABAQUS may produce incorrect results for the sandwich plates with significant core orthotropy [64, 57, 7]. From Fig. 10, it is seen that the core orthotropy has a considerable effect on the buckling loads and their corresponding buckling patterns of the tow-steered sandwich plate, for instance, with the increase of core orthotropy ratio E_{11}^c/E_{33}^c , the buckling load gradually increases in accompany with a sudden transition of the buckling pattern from local instability (antisymmetrical wrinkling) to global instability (global buckling). In particular, the edge wrinkling with multiple halfwaves occurs when the core orthotropy ratio is relatively low, while the global buckling with one single halfwave appears when the core orthotropy ratio is sufficiently significant, as shown in Fig. 10. A similar conclusion can also be drawn from Fig. 11, where a remarkable transition of the buckling pattern from local instability (wrinkling) to coupled instability and finally to global instability (global buckling) is observed with the increase of core orthotropy ratio E_{11}^c/E_{33}^c . These results indicate that the possibility of encountering the wrinkling pattern is greatly increased for a relatively low core orthotropy. It is also noted that there is little difference in the predicted buckling loads between two different boundary conditions when the core orthotropy ratio is relatively low, as shown in Table 2, and the primary reason is attributed to the occurrence of local instability (wrinkling), while this difference becomes significant when the core orthotropy ratio tends to be large.

5.2.3. Effects of fibre orientation angle

The third parametric study mainly focuses on the effect of varying fibre orientation angle of the facesheets on the instability response of VAT sandwich plates, and in particular, the possibility of applying the novel VAT design concept to improve the buckling resistance of the sandwich plate is emphatically explored. Herein, a rectangular sandwich

plate ($a = 200\text{mm}$ and $b = 150\text{mm}$) with SSSS boundary conditions under a uniform end-shortening is considered. The VAT layup configuration of either the top or bottom facesheet is assumed to be $[\phi \pm \langle T_0|T_1 \rangle]_{2s}$, where $\phi = 0^\circ$ or $\phi = 90^\circ$ and both T_0 and T_1 increase from 0° to 90° with a step of 10° . The facesheet thickness is assumed to be $f_t = f_b = 1.0176\text{mm}$, whilst the core thickness is chosen to be $2c = 10\text{mm}$. The material properties of the facesheets are similar to those in the second parametric study, whilst the core is composed of the soft isotropic material, whose properties are given by: $E_{11}^c = E_{22}^c = E_{33}^c = 56\text{MPa}$, $G_{23}^c = G_{13}^c = G_{12}^c = 22\text{MPa}$, $\nu_{23}^c = \nu_{13}^c = \nu_{12}^c = 0.25$. Normalized values of buckling load versus stiffness for various VAT layup configurations with $\phi = 0^\circ$ and $\phi = 90^\circ$ obtained using the present Rayleigh-Ritz model are plotted in Fig. 12 and Fig. 13, respectively, where each curve represents a series of VAT sandwich plates generated by varying the value of T_1 (from 0° at the right-end to 90° at the left-end for the case of $\phi = 0^\circ$ or from 0° at the left-end to 90° at the right-end for the case of $\phi = 90^\circ$) with a same value of T_0 . For the sake of convenience, it is recommended to represent the both the critical buckling load and prebuckling stiffness of the tow-steered sandwich plate in a smeared approach [3]. Herein, the smeared (or averaged) critical buckling load $N_{x,\text{sm}}^{\text{cr}}$ and prebuckling stiffness $E_{x,\text{sm}}$ of the sandwich plate are expressed as [3]:

$$N_{x,\text{sm}}^{\text{cr}} = \frac{\lambda_{\text{cr}}}{b} \int_{-b/2}^{b/2} N_x^0(\pm a/2, y) dy \quad (66a)$$

$$E_{x,\text{sm}} = \frac{a}{hb\Delta_x} \int_{-b/2}^{b/2} N_x^0(\pm a/2, y) dy \quad (66b)$$

For comparison purposes, the smeared critical buckling load and prebuckling stiffness are normalized by the following expression [3]:

$$\overline{N}_{x,\text{sm}}^{\text{cr}} = \frac{N_{x,\text{sm}}^{\text{cr}}}{\max[N_{x,\text{sm}}^{\text{cr}}|_{T_0=T_1}]} \quad (67a)$$

$$\overline{E}_{x,\text{sm}} = \frac{E_{x,\text{sm}}}{\max[E_{x,\text{sm}}]} \quad (67b)$$

From Figs. 12 and 13, it is clear that the instability response of the sandwich plate is significantly affected by the fibre orientation angle, and in particular, the critical buckling load varies with both fibre orientation angles T_0 and T_1 , which makes the VAT sandwich plate possess extended freedom in stiffness tailoring when compared to the straight-fibre composite sandwich plates. Furthermore, for the case of $\phi = 0^\circ$, the buckling loads obtained with VAT layup configurations are found to be enveloped within the curve representing the straight-fibre sandwich plates, as shown in Fig. 12, which means the advantage of applying VAT concept to improve the buckling resistance of the sandwich plate is not obvious for the case of $\phi = 0^\circ$. However, Fig. 13 presents a completely different scenario for the case of $\phi = 90^\circ$, and in particular, it is found that the maximum buckling load is achieved by the VAT layup $[90 \pm \langle 0|70 \rangle]_{2s}$, in which a 23% improvement in the buckling resistance is obtained when compared to the maximum one of the straight-fibre format $[\pm 10]_{2s}$. Actually, the majority of compressive loads within both the top and bottom facesheets are redistributed away from the central region towards the supported edges, which enables the VAT layup $[90 \pm \langle 0|70 \rangle]_{2s}$ to arrive at higher buckling resistance. The distinct superiority of applying the VAT concept enabled by automated fibre placement technologies to improve the stability performance of the sandwich plate is demonstrated.

6. Conclusion

In this paper, a Rayleigh-Ritz analytical model based on a modified version of the EHSAPT was developed for studying the instability behaviour of VAT sandwich plates under in-plane compressive loads. Both global buckling and wrinkling patterns were observed under the present model framework. The proposed three-dimensional sandwich plate model benefits from the introduction of the first-order shear deformation theory into the facesheets, which has shown some advantages such as the conciseness in derivation process and the convenience of modelling implementation. Before instability analysis, the nonuniform prebuckling stresses over the entire sandwich plate were determined under the assumption of membrane prebuckling state. The usage of Lagrange multiplier method in the prebuckling analysis removes the modelling limitations in conventional Rayleigh-Ritz method and thus provides a general way to model in-plane boundary conditions. Comparison studies were firstly conducted to demonstrate the accuracy and effectiveness of the present Rayleigh-Ritz analytical model, and subsequently a series of parametric studies

were provided to investigate the influences of core thickness, core orthotropy, and fibre orientation angle of the facesheets on the instability behaviours of VAT sandwich plates. The results have shown that the change of the core thickness greatly affects the critical buckling load of VAT sandwich plates, and simultaneously triggers a pronounced transition in the instability pattern from global buckling to wrinkling. The core orthotropy has a significant influence on the instability behaviour of the VAT sandwich plates, and in particular, for a relatively low core orthotropy, the possibility of encountering the wrinkling pattern is greatly increased. Moreover, it was observed that the VAT composite sandwich plates exhibits a 23% higher critical buckling load than the straight-fibre format by appropriately selecting VAT pattern over the facesheets. The favorable stress redistribution mechanism that a majority of compressive loads within the facesheets is transferred from the central region to both supported edges was found to be responsible for this significant improvement of the buckling resistance, and the distinct superiority of applying the VAT concept to the sandwich plate was accordingly demonstrated.

Acknowledgments

Xiaodong Chen would like to thank the financial support from the Special Fund for Doctoral Talents (Henan University of Urban Construction, China). Guojun Nie wishes to acknowledge the financial support under the research project from National Natural Science Foundation of China (Nos. 12072239, 11772232, and 11372225). Zhangming Wu wishes to acknowledge the financial support under A3 Talent Research Programme from Ningbo University, China.

References

- [1] C. N. Phan, Y. Frostig, G. A. Kardomateas, Analysis of sandwich beams with a compliant core and with in-plane rigidity—extended high-order sandwich panel theory versus elasticity, *Journal of Applied Mechanics* 79 (2012) 041001.
- [2] V. Birman, G. A. Kardomateas, Review of current trends in research and applications of sandwich structures, *Composites Part B: Engineering* 142 (2018) 221–240.
- [3] B. H. Coburn, P. M. Weaver, Buckling analysis, design and optimisation of variable-stiffness sandwich panels, *International Journal of Solids and Structures* 96 (2016) 217–228.

- [4] R. Vescovini, L. Dozio, A variable-kinematic model for variable stiffness plates: Vibration and buckling analysis, *Composite Structures* 142 (2016) 15–26.
- [5] W. Ji, A. M. Waas, Global and local buckling of a sandwich beam, *Journal of Engineering Mechanics* 133 (2007) 230–237.
- [6] H. Hu, S. Belouettar, M. Potier-Ferry, A. Makradi, A novel finite element for global and local buckling analysis of sandwich beams, *Composite Structures* 90 (2009) 270–278.
- [7] M. D’Ottavio, O. Polit, W. Ji, A. M. Waas, Benchmark solutions and assessment of variable kinematics models for global and local buckling of sandwich struts, *Composite Structures* 156 (2016) 125–134.
- [8] L. A. Carlsson, G. A. Kardomateas, *Structural and failure mechanics of sandwich composites*, Springer, Dordrecht, 1st edition, 2011.
- [9] G. W. Hunt, M. A. Wadee, Localization and mode interaction in sandwich structures, *Proceedings of the Royal Society of London. Series A: Mathematical, Physical and Engineering Sciences* 454 (1998) 1197–1216.
- [10] L. Léotoing, S. Drapier, A. Vautrin, Nonlinear interaction of geometrical and material properties in sandwich beam instabilities, *International Journal of Solids and Structures* 39 (2002) 3717–3739.
- [11] Y. Liu, K. Yu, H. Hu, S. Belouettar, M. Potier-Ferry, N. Damil, A new fourier-related double scale analysis for instability phenomena in sandwich structures, *International Journal of Solids and Structures* 49 (2012) 3077–3088.
- [12] Z. Yuan, G. A. Kardomateas, Nonlinear stability analysis of sandwich wide panels—part ii: Postbuckling response, *Journal of Applied Mechanics* 85 (2018).
- [13] Q. Huang, J. Choe, J. Yang, Y. Hui, R. Xu, H. Hu, An efficient approach for post-buckling analysis of sandwich structures with elastic-plastic material behavior, *International Journal of Engineering Science* 142 (2019) 20–35.
- [14] N. J. Hoff, S. E. Mautner, The buckling of sandwich-type panels, *Journal of the Aeronautical Sciences* 12 (1945) 285–297.

- [15] F. J. Plantema, Sandwich construction, John Wiley & Sons, New York, 1st edition, 1966.
- [16] H. G. Allen, Analysis and Design of Structural Sandwich Panels, Pergamon, London, 1st edition, 1969.
- [17] D. Li, Layerwise theories of laminated composite structures and their applications: A review, Archives of Computational Methods in Engineering 28 (2021) 577–600.
- [18] K. Niu, R. Talreja, Modeling of wrinkling in sandwich panels under compression, Journal of Engineering Mechanics 125 (1999) 875–883.
- [19] Y. Frostig, M. Baruch, High-order buckling analysis of sandwich beams with transversely flexible core, Journal of Engineering Mechanics 119 (1993) 476–495.
- [20] Y. Frostig, M. Baruch, O. Vilnay, I. Sheinman, High-order theory for sandwich-beam behavior with transversely flexible core, Journal of Engineering Mechanics 118 (1992) 1026–1043.
- [21] L. Léotoing, S. Drapier, A. Vautrin, First applications of a novel unified model for global and local buckling of sandwich columns, European Journal of Mechanics - A/Solids 21 (2002) 683–701.
- [22] H. Hu, S. Belouettar, M. Potier-Ferry, A. Makradi, Y. Koutsawa, Assessment of various kinematic models for instability analysis of sandwich beams, Engineering Structures 33 (2011) 572–579.
- [23] K. Yu, H. Hu, H. Tang, G. Giunta, M. Potier-Ferry, S. Belouettar, A novel two-dimensional finite element to study the instability phenomena of sandwich plates, Computer Methods in Applied Mechanics and Engineering 283 (2015) 1117–1137.
- [24] J. Choe, Q. Huang, J. Yang, H. Hu, An efficient approach to investigate the post-buckling behaviors of sandwich structures, Composite Structures 201 (2018) 377–388.
- [25] C. N. Phan, G. A. Kardomateas, Y. Frostig, Global buckling of sandwich beams based on the extended high-order theory, AIAA Journal 50 (2012) 1707–1716.

- [26] C. N. Phan, N. W. Bailey, G. A. Kardomateas, M. A. Battley, Wrinkling of sandwich wide panels/beams based on the extended high-order sandwich panel theory: formulation, comparison with elasticity and experiments, *Archive of Applied Mechanics* 82 (2012) 1585–1599.
- [27] Y. Frostig, V. Birman, G. A. Kardomateas, Non-linear wrinkling of a sandwich panel with functionally graded core – extended high-order approach, *International Journal of Solids and Structures* 148-149 (2018) 122–139.
- [28] Z. Yuan, G. A. Kardomateas, Nonlinear stability analysis of sandwich wide panels—part i: Buckling behavior, *Journal of Applied Mechanics* 85 (2018).
- [29] A. Bakoura, F. Bourada, A. A. Bousahla, A. Tounsi, K. H. Benrahou, A. Tounsi, M. M. Al-Zahrani, S. R. Mahmoud, Buckling analysis of functionally graded plates using hsdts in conjunction with the stress function method, *Computers and Concrete* 27 (2021) 73–83.
- [30] S. I. Tahir, A. Chikh, A. Tounsi, M. A. Al-Osta, S. U. Al-Dulaijan, M. M. Al-Zahrani, Wave propagation analysis of a ceramic-metal functionally graded sandwich plate with different porosity distributions in a hygro-thermal environment, *Composite Structures* 269 (2021) 114030.
- [31] M. W. Zaitoun, A. Chikh, A. Tounsi, M. A. Al-Osta, A. Sharif, S. U. Al-Dulaijan, M. M. Al-Zahrani, Influence of the visco-pasternak foundation parameters on the buckling behavior of a sandwich functional graded ceramic–metal plate in a hygrothermal environment, *Thin-Walled Structures* 170 (2022) 108549.
- [32] A. Rachid, D. Ouinas, A. Lousdad, F. Z. Zaoui, B. Achour, H. Gasmi, T. A. Butt, A. Tounsi, Mechanical behavior and free vibration analysis of fg doubly curved shells on elastic foundation via a new modified displacements field model of 2d and quasi-3d hsdts, *Thin-Walled Structures* 172 (2022) 108783.
- [33] D. J. Dawe, W. X. Yuan, Overall and local buckling of sandwich plates with laminated faceplates, part i: Analysis, *Computer Methods in Applied Mechanics and Engineering* 190 (2001) 5197–5213.

- [34] J. B. Dafedar, Y. M. Desai, A. A. Mufti, Stability of sandwich plates by mixed, higher-order analytical formulation, *International Journal of Solids and Structures* 40 (2003) 4501–4517.
- [35] J. Hohe, L. Librescu, S. Yong Oh, Dynamic buckling of flat and curved sandwich panels with transversely compressible core, *Composite Structures* 74 (2006) 10–24.
- [36] M. M. Kheirikhah, S. M. R. Khalili, K. Malekzadeh Fard, Biaxial buckling analysis of soft-core composite sandwich plates using improved high-order theory, *European Journal of Mechanics - A/Solids* 31 (2012) 54–66.
- [37] M.-A. Douville, P. Le Grogneq, Exact analytical solutions for the local and global buckling of sandwich beam-columns under various loadings, *International Journal of Solids and Structures* 50 (2013) 2597–2609.
- [38] E. Carrera, Theories and finite elements for multilayered, anisotropic, composite plates and shells, *Archives of Computational Methods in Engineering* 9 (2002) 87–140.
- [39] E. Carrera, S. Brischetto, A survey with numerical assessment of classical and refined theories for the analysis of sandwich plates, *Applied Mechanics Reviews* 62 (2008).
- [40] L. Demasi, ∞^3 hierarchy plate theories for thick and thin composite plates: The generalized unified formulation, *Composite Structures* 84 (2008) 256–270.
- [41] L. Demasi, 2d, quasi 3d and 3d exact solutions for bending of thick and thin sandwich plates, *Journal of Sandwich Structures & Materials* 10 (2008) 271–310.
- [42] R. Vescovini, M. D’Ottavio, L. Dozio, O. Polit, Buckling and wrinkling of anisotropic sandwich plates, *International Journal of Engineering Science* 130 (2018) 136–156.
- [43] Z. Gürdal, B. Tatting, C. Wu, Variable stiffness composite panels: Effects of stiffness variation on the in-plane and buckling response, *Composites Part A: Applied Science and Manufacturing* 39 (2008) 911–922.
- [44] Z. Wu, P. M. Weaver, G. Raju, B. C. Kim, Buckling analysis and optimisation of variable angle tow composite plates, *Thin Walled Structures* 60 (2012) 163–172.

- [45] Z. Wu, G. Raju, P. M. Weaver, Postbuckling analysis of variable angle tow plates, *International Journal of Solids and Structures* 50 (2013) 1770–1780.
- [46] G. Raju, Z. Wu, B. Kim, P. M. Weaver, Prebuckling and buckling analysis of variable angle tow plates with general boundary conditions, *Composite Structures* 94 (2012) 2961–2970.
- [47] G. Raju, Z. Wu, P. M. Weaver, Postbuckling analysis of variable angle tow plates using differential quadrature method, *Composite Structures* 106 (2013) 74–84.
- [48] Z. Wu, G. Raju, P. M. Weaver, Framework for the buckling optimization of variable angle tow composite plates, *AIAA Journal* 53 (2015) 3788–3804.
- [49] P. Hao, C. Liu, X. Yuan, B. Wang, G. Li, T. Zhu, F. Niu, Buckling optimization of variable-stiffness composite panels based on flow field function, *Composite Structures* 181 (2017) 240–255.
- [50] X. Chen, Z. Wu, G. Nie, P. Weaver, Buckling analysis of variable angle tow composite plates with a through-the-width or an embedded rectangular delamination, *International Journal of Solids and Structures* 138 (2018) 166–180.
- [51] X. Chen, G. Nie, Prebuckling and buckling analysis of moderately thick variable angle tow composite plates considering the extension-shear coupling, *Composite Structures* 242 (2020) 112093.
- [52] X. Chen, G. Nie, Z. Wu, Application of Rayleigh-Ritz formulation to thermomechanical buckling of variable angle tow composite plates with general in-plane boundary constraint, *International Journal of Mechanical Sciences* 187 (2020) 106094.
- [53] X. Chen, G. Nie, X. Yang, Thermal postbuckling analysis of variable angle tow composite cylindrical panels, *Journal of Thermal Stresses* 44 (2021) 850–882.
- [54] J. N. Reddy, *Mechanics of laminated composite plates and shells theory and analysis*, CRC Press, New York, 2nd edition, 2004.
- [55] R. Vescovini, L. Dozio, M. D’Ottavio, O. Polit, On the application of the ritz method to free vibration and buckling analysis of highly anisotropic plates, *Composite Structures* 192 (2018) 460–474.

- [56] Z. Wu, G. Raju, P. M. Weaver, Buckling of vat plates using energy methods, in: 53rd AIAA/ASME/ASCE/AHS/ASC Structures, Structural Dynamics and Materials Conference, AIAA 2012-1463, Honolulu, Hawaii.
- [57] W. Ji, A. M. Waas, Accurate buckling load calculations of a thick orthotropic sandwich panel, *Composites Science and Technology* 72 (2012) 1134–1139.
- [58] H. Huang, G. A. Kardomateas, Buckling and initial postbuckling behavior of sandwich beams including transverse shear, *AIAA Journal* 40 (2002) 2331–2335.
- [59] Z. P. Bažant, A. Beghini, Stability and finite strain of homogenized structures soft in shear: Sandwich or fiber composites, and layered bodies, *International Journal of Solids and Structures* 43 (2006) 1571–1593.
- [60] W. Ji, A. M. Waas, 2d elastic analysis of the sandwich panel buckling problem: benchmark solutions and accurate finite element formulations, *Zeitschrift für angewandte Mathematik und Physik* 61 (2010) 897–917.
- [61] L. Fagerberg, Wrinkling and compression failure transition in sandwich panels, *Journal of Sandwich Structures & Materials* 6 (2004) 129–144.
- [62] L. Fagerberg, D. Zenkert, Effects of anisotropy and multiaxial loading on the wrinkling of sandwich panels, *Journal of Sandwich Structures & Materials* 7 (2005) 177–194.
- [63] C. A. Rose, D. F. Moore, N. F. Knight, C. C. Rankin, Finite element modeling of the buckling response of sandwich panels, in: 43rd AIAA/ASME/ASCE/AHS/ASC Structures, Structural Dynamics, and Materials Conference, AIAA 2002-1517, Denver, Colorado, pp. 1–19.
- [64] W. Ji, A. M. Waas, Z. P. Bažant, Errors caused by non-work-conjugate stress and strain measures and necessary corrections in finite element programs, *Journal of Applied Mechanics* 77 (2010).

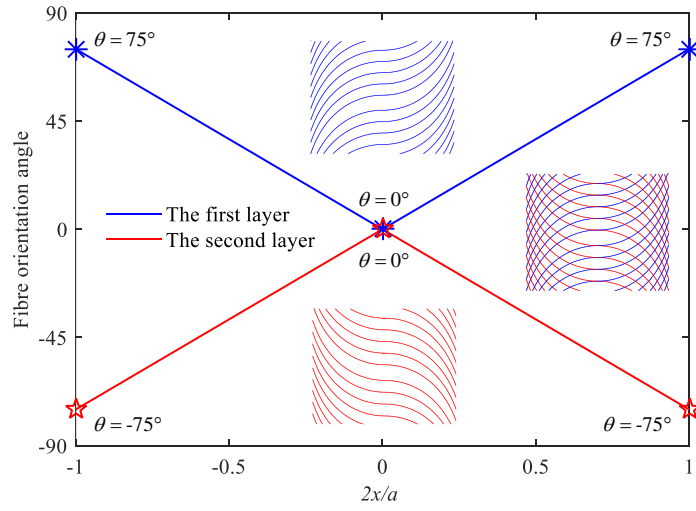


Figure 1: A two-layers VAT facesheet $[0 \pm \langle 0|75 \rangle]$ with a linear variation of fibre orientation angle ($\phi = 0^\circ$, $T_0 = 0^\circ$, and $T_1 = 75^\circ$).

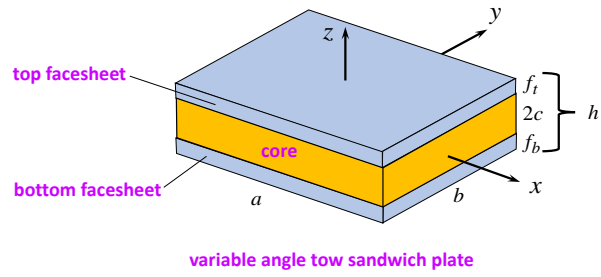


Figure 2: Schematic diagram of a typical VAT sandwich plate with two facesheets and one core. (The orthogonal coordinate system is located in the centroid of the core)

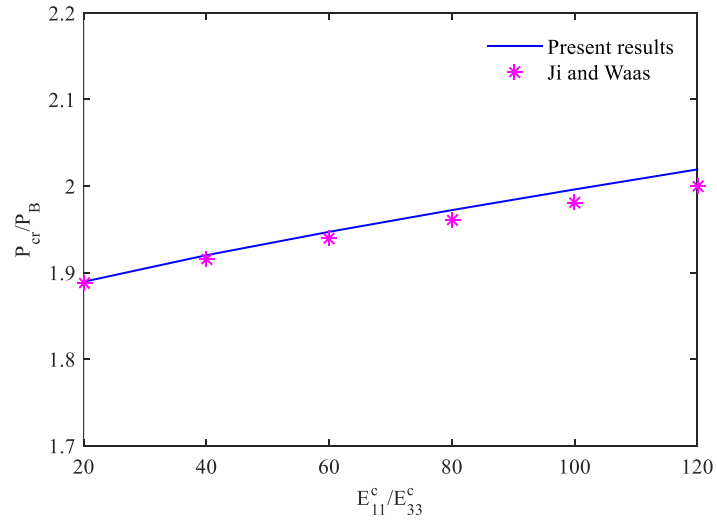


Figure 3: Comparison of the normalized critical buckling load between the present results and the previously published results for a short sandwich beam with different orthotropy ratios E_{11}^c/E_{33}^c .

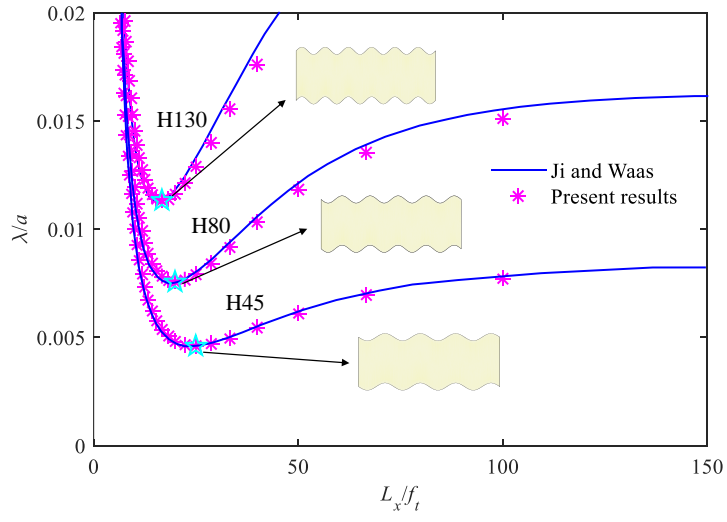


Figure 4: Comparison of the normalized critical strain λ/a versus the normalized half-wavelength L_x/f_t between the present results and the previously published results for a symmetrical sandwich wide beam with three different cores, that is, H45, H80, and H130.

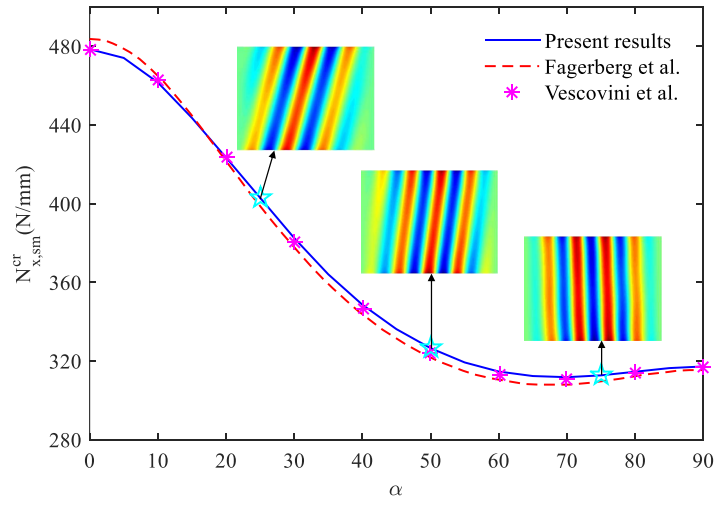


Figure 5: Comparison of the critical buckling load ($N_{x,sm}^{cr}$) between the present results and the previously published results for a rectangular sandwich plate with different rotation angles (α). (unit: N/mm)

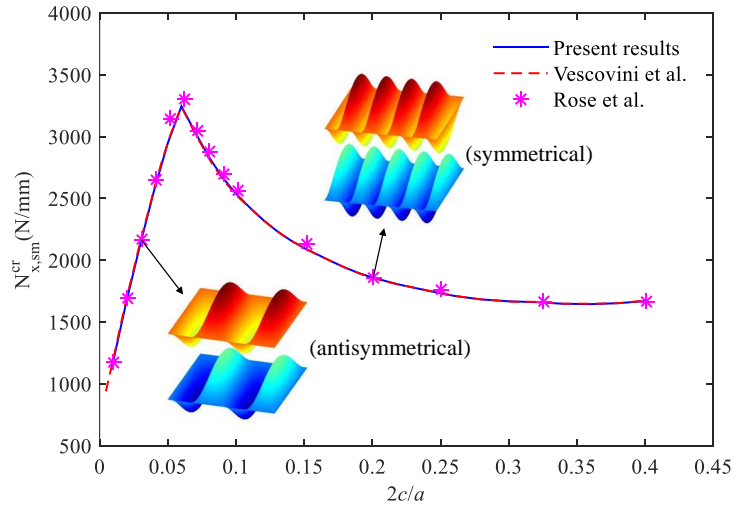


Figure 6: Comparison of the critical buckling load ($N_{x,sm}^{cr}$) between the present results and the previously published results for a rectangular sandwich plate with different values of normalized core thickness ($2c/a$). (unit: N/mm)

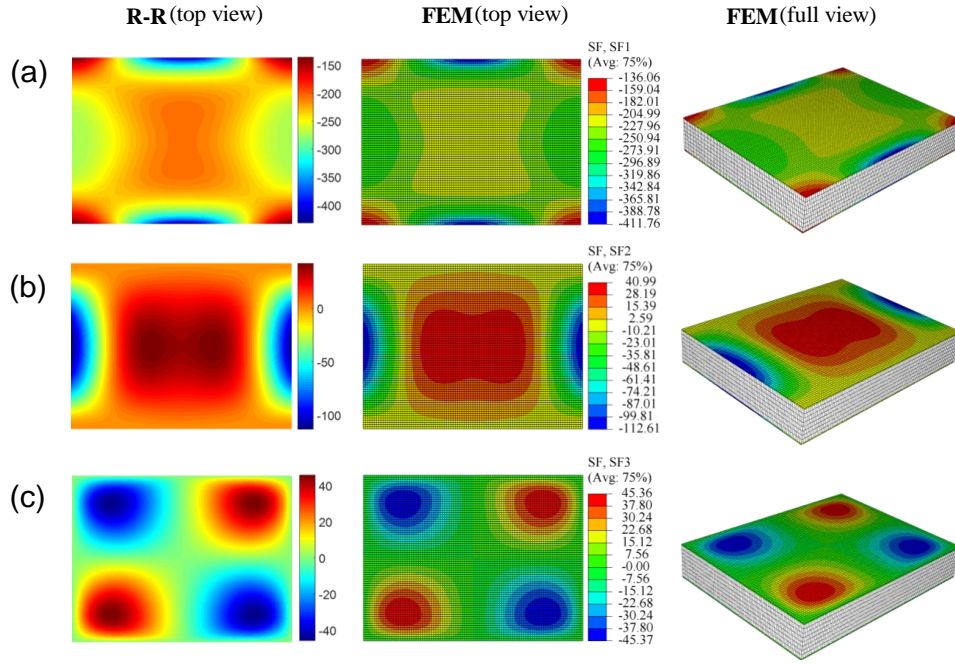


Figure 7: Comparison of FEM and Rayleigh–Ritz results on the nonuniform prebuckling stress distribution of the top facesheet within the VAT sandwich plate $[\pm(0|45)]_s$ under uniform end shortening ($\Delta_x = 0.5\text{mm}$) with transverse edges free to deform: (a) longitudinal stress resultant \hat{N}_{xx}^t ; (b) transverse stress resultant \hat{N}_{yy}^t ; (c) in-plane shear stress resultant \hat{N}_{xy}^t .

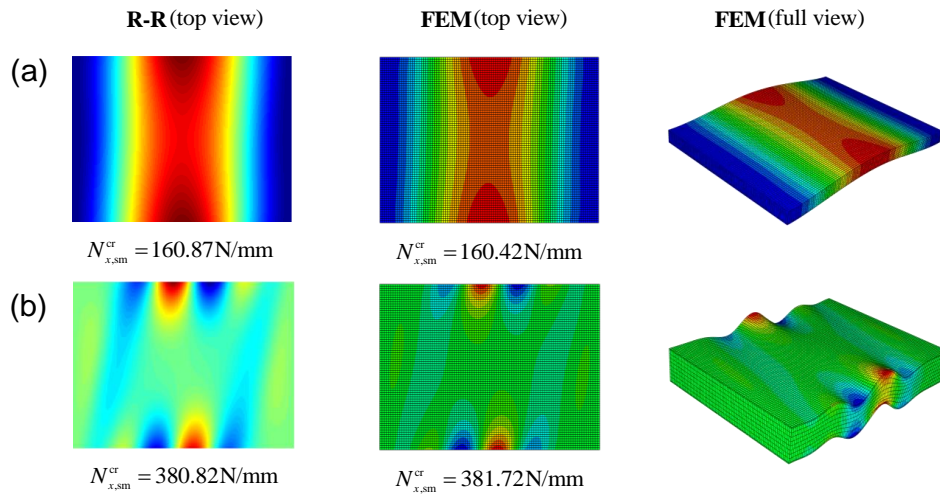


Figure 8: Comparison of FEM and Rayleigh–Ritz results on the critical buckling loads and the corresponding instability patterns of the VAT sandwich plate $[\pm\langle 0|45\rangle]_s$ under uniform end shortening with transverse edges free to deform: (a) $2c = 10\text{mm}$; (b) $2c = 30\text{mm}$.

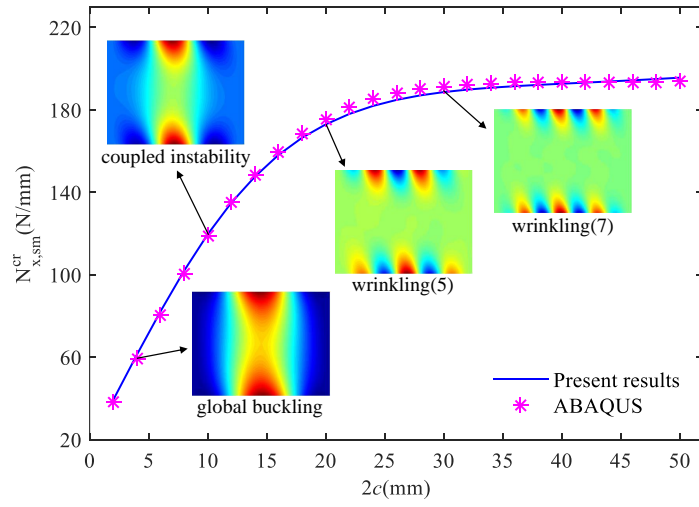


Figure 9: The critical buckling load ($N_{x,sm}^{cr}$) as a function of the core thickness ($2c$) of the VAT sandwich plate $[90 \pm (0|75)]_s$ under uniform end shortening (The results obtained using ABAQUS are also included for comparison purposes). (unit: N/mm)

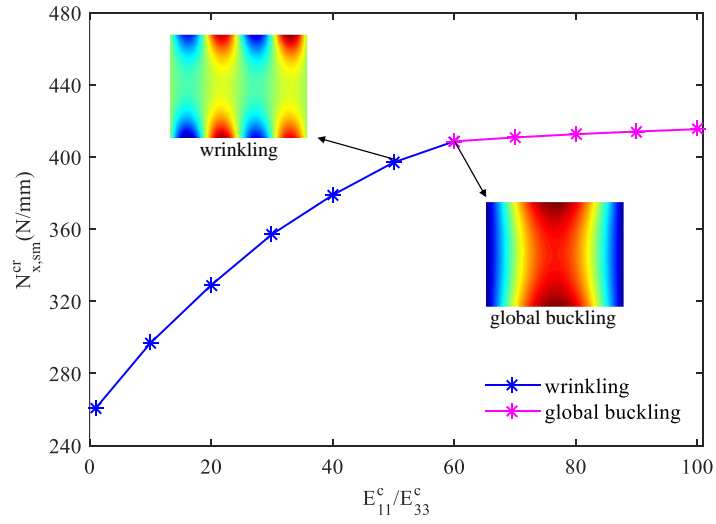


Figure 10: The critical buckling load ($N_{x,sm}^{cr}$) as a function of the core orthotropy (E_{11}^c/E_{33}^c) of the VAT sandwich plate $[90 \pm \langle 0|75 \rangle]_s$ with SFSF boundary conditions under uniform end shortening. (unit: N/mm)

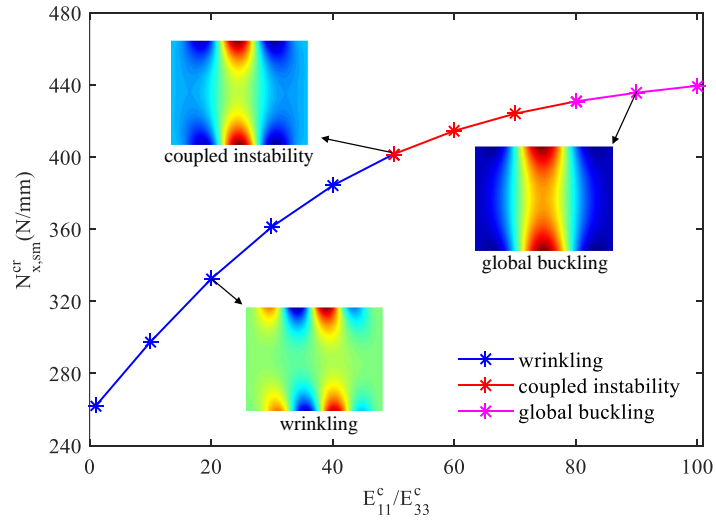


Figure 11: The critical buckling load ($N_{x,sm}^{cr}$) as a function of the core orthotropy (E_{11}^c/E_{33}^c) of the VAT sandwich plate $[90 \pm \langle 0|75 \rangle]_s$ with CFCF boundary conditions under uniform end shortening. (unit: N/mm)

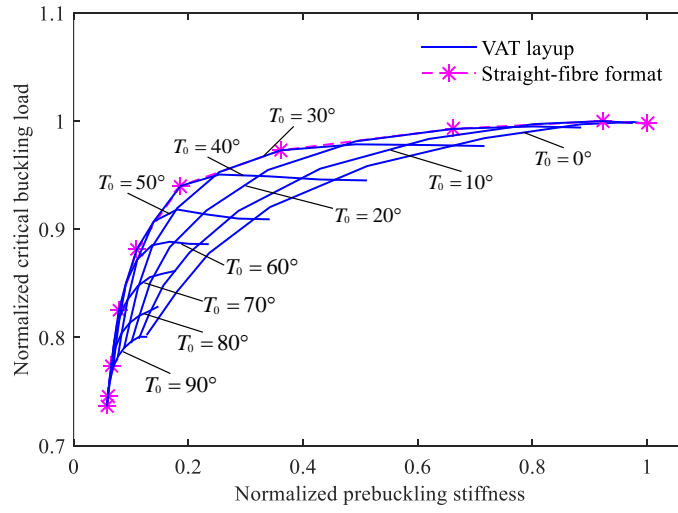


Figure 12: Normalized buckling load versus normalized prebuckling stiffness of the VAT sandwich plates with all the VAT configurations $[\phi \pm \langle T_0 | T_1 \rangle]_{2s}$ under uniform end-shortening for the case of $\phi = 0$.

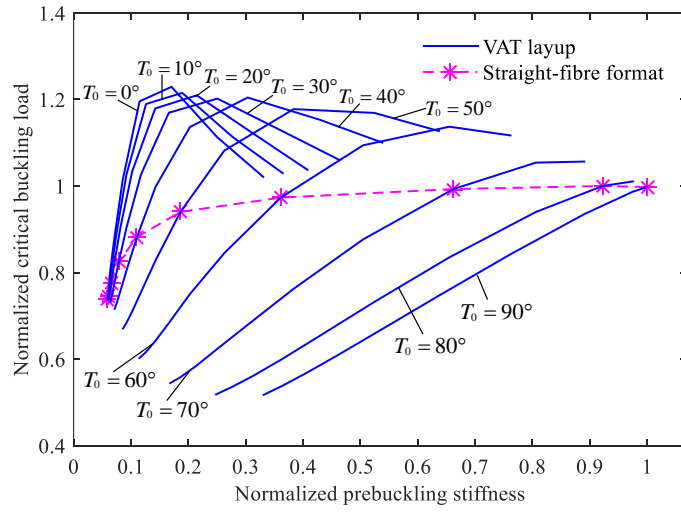


Figure 13: Normalized buckling load versus normalized prebuckling stiffness of the VAT sandwich plates with all the VAT configurations $[\phi \pm \langle T_0 | T_1 \rangle]_{2s}$ under uniform end-shortening for the case of $\phi = 90^\circ$.